Article

Cell Reports

HP1 Is Involved in Regulating the Global Impact of DNA Methylation on Alternative Splicing

Graphical Abstract

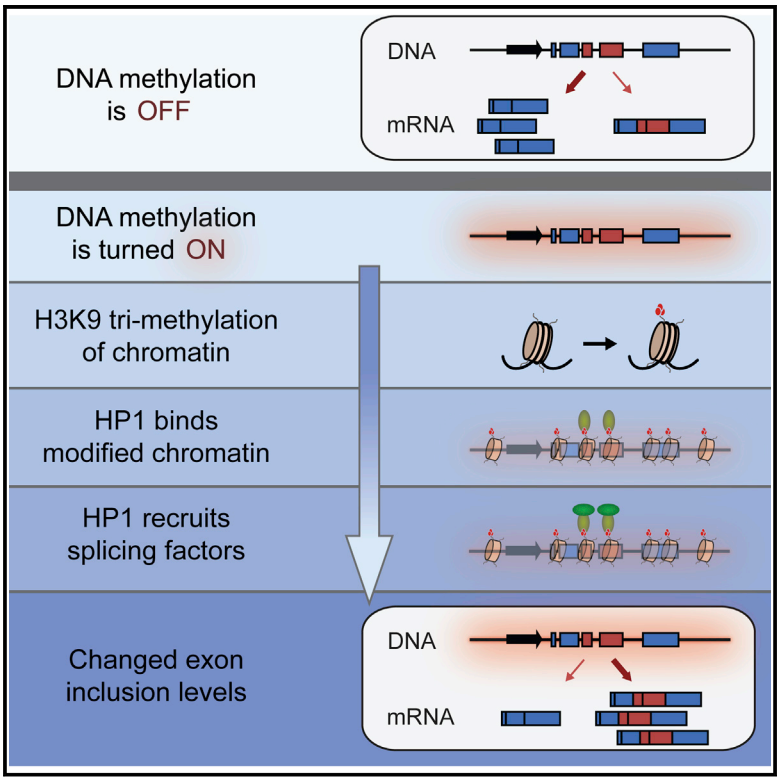

Authors

Ahuvi Yearim, Sahar Gelfman, ..., Eran Meshorer, Gil Ast

Correspondence

meshorer@huji.ac.il (E.M.), gilast@post.tau.ac.il (G.A.)

In Brief

The global impact of DNA methylation on mRNA splicing is largely unknown. Yearim et al. characterize the genome-wide effect of DNA methylation on alternative splicing and demonstrate a direct relationship between DNA methylation and splicing. Additionally, they describe an adaptor system for splicing factor recruitment by DNA methylation through HP1 proteins.

Highlights

- DNA methylation directly affects mRNA alternative splicing
- Methylation-affected exons display distinct genetic and epigenetic signatures
- HP1 mediates DNA methylation's effect on splicing by recruiting splicing factors
- HP1 enhances or silences inclusion depending on its relative binding position

Accession Numbers

GSE64910

Yearim et al., 2015, Cell Reports *10*, 1–13
February 24, 2015
http://dx.doi.org/10.1016/j.celrep.2015.01.038

CellPress

Please cite this article in press as: Yearim et al., HP1 Is Involved in Regulating the Global Impact of DNA Methylation on Alternative Splicing, Cell Reports (2015), http://dx.doi.org/10.1016/j.celrep.2015.01.038

Cell Reports
Article

HP1 Is Involved in Regulating the Global Impact of DNA Methylation on Alternative Splicing

Ahuvi Yearim,[1,5] Sahar Gelfman,[1,4,5] Ronna Shayevitch,[1] Shai Melcer,[2] Ohad Glaich,[1] Jan-Philipp Mallm,[3] Malka Nissim-Rafinia,[2] Ayelet-Hashahar S. Cohen,[2] Karsten Rippe,[3] Eran Meshorer,[2,6,*] and Gil Ast[1,6,*]
[1]Department of Human Molecular Genetics and Biochemistry, Sackler Faculty of Medicine, Tel-Aviv University, Ramat Aviv 69978, Israel
[2]Department of Genetics, Institute of Life Sciences, The Hebrew University of Jerusalem, Edmond J. Safra (Givat Ram) Campus, Jerusalem 91904, Israel
[3]Deutsches Krebsforschungszentrum (DKFZ) and BioQuant, Research Group Genome Organization & Function, Im Neuenheimer Feld 280, 69120 Heidelberg, Germany
[4]Center for Human Genome Variation, Duke University School of Medicine, Durham, NC 27708, USA
[5]Co-first author
[6]Co-senior author
*Correspondence: meshorer@huji.ac.il (E.M.), gilast@post.tau.ac.il (G.A.)
http://dx.doi.org/10.1016/j.celrep.2015.01.038

SUMMARY

The global impact of DNA methylation on alternative splicing is largely unknown. Using a genome-wide approach in wild-type and methylation-deficient embryonic stem cells, we found that DNA methylation can either enhance or silence exon recognition and affects the splicing of more than 20% of alternative exons. These exons are characterized by distinct genetic and epigenetic signatures. Alternative splicing regulation of a subset of these exons can be explained by heterochromatin protein 1 (HP1), which silences or enhances exon recognition in a position-dependent manner. We constructed an experimental system using site-specific targeting of a methylated/unmethylated gene and demonstrate a direct causal relationship between DNA methylation and alternative splicing. HP1 regulates this gene's alternative splicing in a methylation-dependent manner by recruiting splicing factors to its methylated form. Our results demonstrate DNA methylation's significant global influence on mRNA splicing and identify a specific mechanism of splicing regulation mediated by HP1.

INTRODUCTION

DNA methylation is an important epigenetic mark, significantly contributing to natural human variation (Heyn et al., 2013). Examination of the full DNA methylome revealed that DNA methylation has dual and opposing roles in the regulation of gene expression. In promoter regions, DNA methylation is associated with transcriptional repression, while in gene bodies, DNA methylation is generally associated with high expression levels (Ball et al., 2009; Laurent et al., 2010; Rauch et al., 2009). The understanding that DNA methylation is significantly present in the bodies of highly transcribed genes led to speculation about its possible biological role in transcription or subsequent processing of active genes.

Alternative splicing contributes to proteome diversity. At least 95% of human multi-exon genes produce alternatively spliced transcripts (Pan et al., 2008; Wang et al., 2008). High-resolution bisulfite sequencing of the genomes of several organisms showed an enrichment of DNA methylation in exons compared to introns (Chodavarapu et al., 2010; Hodges et al., 2009; Lyko et al., 2010). In addition, we previously found that gene regions encoding constitutively spliced exons display higher levels of methylation than those encoding alternatively spliced exons (Gelfman et al., 2013). DNA methylation was also recently found to be positively correlated with inclusion levels of alternative exons (Maunakea et al., 2013). These correlations prompted speculation that DNA methylation plays a role in the regulation of alternative splicing.

Given the fact that splicing occurs co-transcriptionally, there are two possible models for epigenetic regulation of splicing: (1) a kinetic model, in which an epigenetic modification affects the kinetics of transcriptional elongation that subsequently impacts splicing, and (2) a recruitment model, in which splicing regulation occurs through adaptor proteins that bind to epigenetic modifications and recruit splicing factors (Iannone and Valcárcel, 2013). Several recent studies now support methylation-regulated splicing via a kinetic model. Transcriptional repressors such as CTCF and MeCP2 were found to modify the elongation rate of RNA polymerase II (RNAPII) in a methylation-dependent manner, which in turn enhances (MeCP2) or disturbs (CTCF) the efficiency of splicing (Maunakea et al., 2013; Shukla et al., 2011). In support of the recruitment model for other epigenetic modifications, the histone modification H3K36me3 was found to recruit the splicing factors PTB (Luco et al., 2010) and SRSF1 (Pradeepa et al., 2012). However, to date, DNA methylation has not been found to participate in any recruitment mechanism that affects splicing.

For DNA methylation to regulate splicing, it likely has a mediator protein that can affect splicing regulation on the one hand

Please cite this article in press as: Yearim et al., HP1 Is Involved in Regulating the Global Impact of DNA Methylation on Alternative Splicing, Cell Reports (2015), http://dx.doi.org/10.1016/j.celrep.2015.01.038

and is selective to DNA methylation on the other. One promising candidate is heterochromatin protein 1 (HP1), which has three isoforms in humans: HP1α, HP1β, and HP1γ. All HP1 proteins bind directly via their chromodomains to H3K9me3 (Bannister et al., 2001; Jacobs and Khorasanizadeh, 2002), a histone modification that is induced by DNA methylation (Hashimshony et al., 2003). Some HP1 isoforms have been previously linked to splicing regulation in specific cases (Alló et al., 2009; Ameyar-Zazoua et al., 2012; Saint-André et al., 2011; Schor et al., 2013; Smallwood et al., 2012). The combined evidence that HP1 can act as a splicing regulator in some contexts and also associates with H3K9me3, a histone modification that is co-localized with regions of methylated DNA, makes HP1 a potential candidate protein that regulates alternative splicing in a methylation-dependent manner.

Given that DNA methylation plays a role in the regulation of mRNA splicing, a whole-genome analysis can decipher the extent and magnitude of the global impact of DNA methylation on splicing and uncover underlying trends and patterns. To what extent does DNA methylation affect splicing? Does it affect all exons or only a specific group with specific characteristics? Also, do HP1 proteins work in concert with methylation to create a combined regulatory effect? To address these questions and more, we used a genome-wide approach and found that more than 20% of all alternative exons are affected by the absence of DNA methylation; for these exons, DNA methylation acts as either an enhancer or a silencer of splicing recognition. We characterized these methylation-affected exons and found that they possess specific genetic and epigenetic signatures that distinguish them from other exons. We applied our genome-wide approach to analyze the effect of HP1 proteins on splicing and found that these proteins also affect the inclusion level of a large amount of alternative exons, again acting as either splicing enhancers or silencers depending on the context of their binding to the exon. Splicing regulation through HP1 explains a significant portion of the overall effect of DNA methylation on splicing. To validate these findings, we established a novel experimental system that specifically targets DNA methylation to a single gene, and to that gene alone, and offer the first clear evidence that DNA methylation regulates alternative splicing directly, acting as a splicing enhancer in this case. HP1 also regulates alternative splicing in this system and acts as a splicing silencer. Finally, we decipher HP1's regulatory mechanism and provide a strong link between DNA methylation and alternative splicing via a recruitment model, i.e., by recruiting splicing factors to methylated alternative exons through an adaptor protein, HP1.

RESULTS

Altered DNA Methylation Patterns Affect Alternative Splicing Globally

The emerging picture from previous studies supports an important link between DNA methylation and splicing (Gelfman et al., 2013; Maunakea et al., 2013; Shukla et al., 2011). However, the extent and magnitude of this impact and its underlying trends and patterns are still not fully known. To address this issue, we performed RNA sequencing (RNA-seq) experiments on wild-type (R1) and Dnmt1/3a/3b triple-knockout (TKO) mouse embryonic stem cells (ESCs) that lack DNA methyltransferase activity, which results in unmethylated DNA in these cells (Melcer et al., 2012; Tsumura et al., 2006). The TKO cells continue to grow robustly, maintain their undifferentiated characteristics, and display morphological features similar to wild-type undifferentiated ESCs (Tsumura et al., 2006). We determined the inclusion levels of 14,987 alternative cassette exons in each cell type using RNA-seq. We next filtered the results based on very stringent read-depth criteria (see Supplemental Experimental Procedures). Of 3,376 alternative exons that met our criteria, inclusion levels of 752 (22.2%) differed by more than 10% in TKO compared to wild-type cells: 271 exons (8% of all alternative exons) decreased their inclusion level in TKO cells, which means that they were positively affected by methylation in the wild-type cells, and 481 exons (14.2% of all alternative exons) increased their inclusion level in TKO cells and thus were negatively affected by methylation in the wild-type (Figures 1A and S1A). These results indicate that DNA methylation can influence alternative splicing in both directions, having both positive (enhancing) and negative (silencing) roles in exon recognition. RT-PCR analysis of selected exons further validated these findings, supporting RNA-seq results in 93% of the cases (Figure S1B). We analyzed RNA expression levels of all spliceosome components in wild-type and TKO cells and found no significant changes (Table S1), implying that most of the changes in alternative splicing in TKO cells are a direct outcome of DNA methylation removal and not variations in quantities of splicing factors. We also performed differential expression analyses between wild-type and TKO cells for all mouse genes, revealing only minor overall differences in expression (Table S2). This finding fits well with previous knowledge that in mouse ESCs, CpG island promoters are not usually repressed by DNA methylation and are instead silenced by H3K27 methylation (Smith and Meissner, 2013).

To study the connection between a methylation-related effect and DNA methylation signal patterns, we performed whole-genome bisulfite sequencing at 10× coverage in wild-type R1 cells and mapped the methylation profile at single-base resolution. We then examined methylation levels in exons and their flanking intronic regions. Constitutive exons exhibited high methylation levels, whereas alternative exons, in general, exhibited lower levels of methylation (Figure 1B), as was also shown previously (Gelfman et al., 2013). This can imply that DNA methylation promotes exon inclusion, but our results suggest that the underlying mechanism is more complex. Constitutive exons in wild-type cells remain constitutive for the most part in TKO cells (98.5% of exons; data not shown), probably since their sequence-based splicing signals strongly support recognition by the splicing machinery, overshadowing the weaker DNA methylation effect. However, alternative exons that are more sensitive to regulation by DNA methylation show different levels of DNA methylation (Figure 1B). Exons that were negatively affected by methylation had significantly higher levels of methylation than positively affected exons (+40%–50% exonic; t test, p value < 3.24×10^{-10}), while alternative exons unaffected by methylation were found exactly between these two groups, with intermediate methylation values. This result suggests that when the exonic splicing signals are weaker (as is the case with alternative exons)

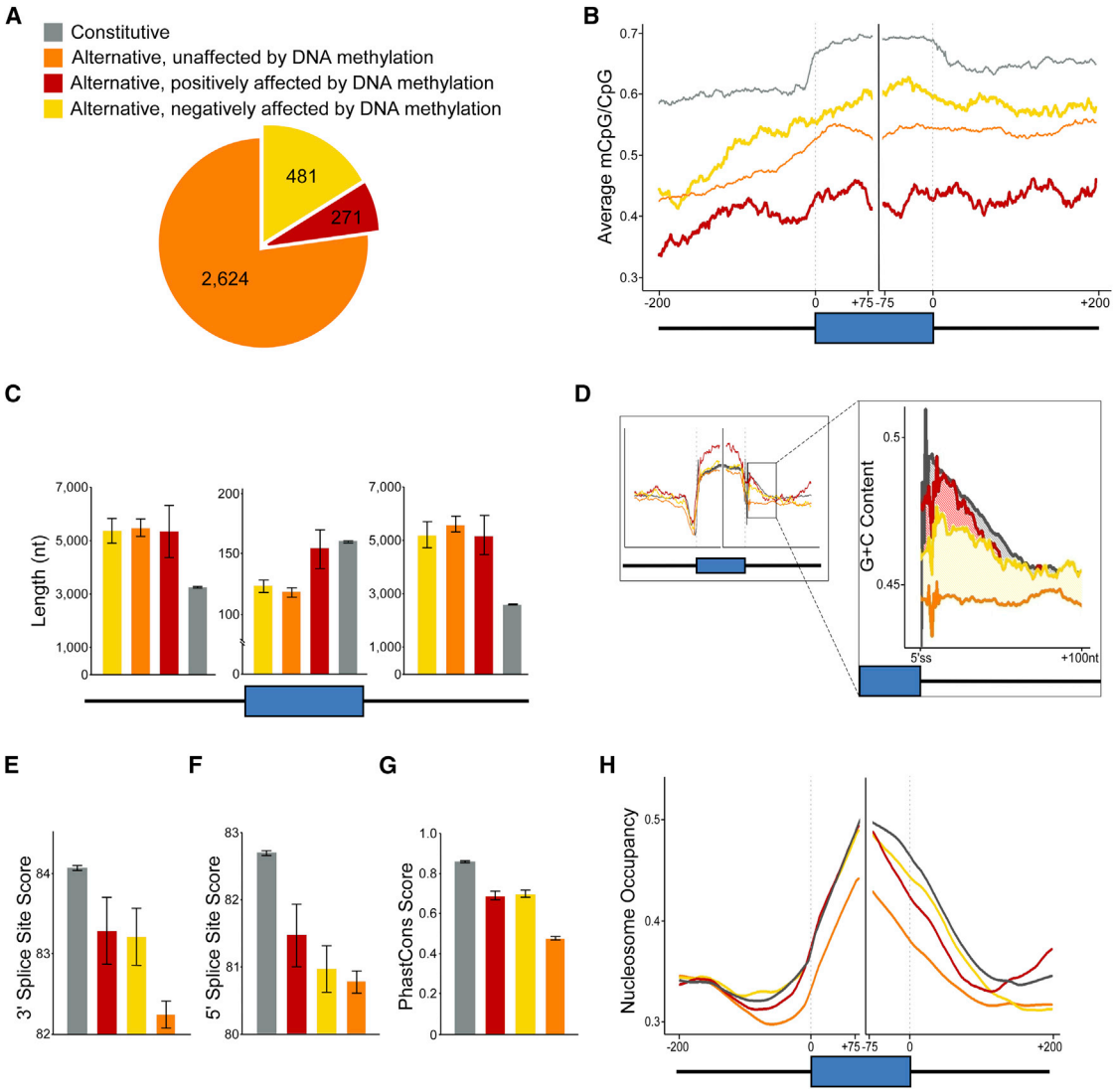

Figure 1. The Global Effect of DNA Methylation on Splicing Regulation

(A) Distribution of alternative exons based on direction of change in splicing pattern from TKO (unmethylated) to R1 (methylated) cells.

(B) Average of methylated CpGs for alternative (three groups) and constitutive exons.

(C) Average length of upstream introns (left), exons (center), and downstream introns (right) for alternative (three groups) and constitutive exons.

(D) G+C content for alternative (three groups) and constitutive exons. Right panel is a close-up of the first 100 nt downstream of the 5′ splice site (5′ss).

(E) Average score of the 3′ splice sites for alternative (three groups) and constitutive exons based on a PSSM calculation (Amit et al., 2012).

(F) Average score of the 5′ splice sites for alternative (three groups) and constitutive exons.

(G) PhastCons conservation values for alternative (three groups) and constitutive exons. Error bars represent the SEM.

(H) Nucleosome occupancy in R1 cells for alternative (three groups) and constitutive exons.

The average values given in (B), (D), and (H) were calculated per base for exons (75 nt from each splice site) and flanking intronic regions (200 nt), and a running average was applied. See also Figure S1.

and the recognition of the exon is not strongly controlled by the basic splicing recognition factors, DNA methylation allows the fine-tuning of this recognition. In this case, high methylation levels will repress recognition of exons, while low methylation levels will enhance their recognition.

We next sought to better understand what defines the subgroups of exons that are regulated by DNA methylation. Interestingly, exons affected by methylation, especially those with higher levels of inclusion in wild-type cells, show a resemblance to constitutively spliced exons in several attributes. Usually, the average length of alternatively spliced exons is relatively short compared to constitutive exons (Gelfman et al., 2012). However, exons that are included in a methylation-dependent manner are longer, with an average length comparable to constitutive exons (Figure 1C). Moreover, similarly to constitutive exons, methylation-dependent exons have a high G+C content signal

Please cite this article in press as: Yearim et al., HP1 Is Involved in Regulating the Global Impact of DNA Methylation on Alternative Splicing, Cell Reports (2015), http://dx.doi.org/10.1016/j.celrep.2015.01.038

downstream of the 5′ splice site, whereas exons unaffected by methylation do not (Figure 1D). This downstream G+C signal was previously shown to have a splicing regulatory role (Amit et al., 2012). Last, all methylation-affected exons possess stronger 3′ splice sites than those unaffected by methylation, again more in resemblance to constitutive exons (Figure 1E). This difference in splice site strength was found mainly in 3′ splice sites and was not pronounced for 5′ splice sites, suggesting that it is not a result of G+C structure at the splice site (Figure 1F). This overall resemblance places exons that are regulated by DNA methylation on the scale of several factors somewhere in between unaffected alternative exons and constitutively spliced exons. Overall, alternative exons whose recognition is sensitive to DNA methylation appear to possess particularly strong factors for recognition yet are not strong enough to overcome the fine-tuned regulation by methylation (as is the case with constitutive exons).

We investigated evolutionary conservation of the different exons that are either regulated or unaffected by DNA methylation (see Supplemental Experimental Procedures). Interestingly, we found that methylation-affected exons are significantly more conserved than methylation unaffected exons (Figure 1G; Mann-Whitney test, p value $< 2.2 \times 10^{-16}$ and p value $= 2.8 \times 10^{-11}$ for negatively and positively affected exons, respectively). This finding highlights the biological importance of alternative exons that are regulated by DNA methylation, as they appear to be under higher selective pressure compared to other alternative exons.

We and others previously observed a correlation between nucleosome occupancy and exon recognition (Schwartz et al., 2009; Tilgner et al., 2009), and DNA methylation was recently shown to regulate nucleosome occupancy (Huff and Zilberman, 2014). To examine the possible role of nucleosome occupancy levels in methylation-dependent exons, we performed MNase-sequencing experiments to map nucleosome occupancy in the various exon groups. Alternative exons unaffected by methylation displayed a weaker nucleosome signal than did constitutive exons, as was previously observed for alternative exons in general (Schwartz et al., 2009; Tilgner et al., 2009). However, methylation-dependent alternative exons displayed levels of nucleosome occupancy similar to those of constitutive exons in both wild-type and TKO cells (Figures 1H and S1C, respectively). This result supports the previous claim, which places exons that are regulated by DNA methylation somewhere in between unaffected skipped exons and the highly recognized constitutively spliced exons.

Since DNA methylation can modulate RNAPII kinetics (Maunakea et al., 2013; Shukla et al., 2011), we asked whether this is also the case for our methylation-affected exons. We examined RNAPII occupancy using publicly available chromatin immunoprecipitation sequencing (ChIP-seq) data from mouse ESCs (Tiwari et al., 2012). The results exhibit a strong accumulation of RNAPII immediately upstream of positively affected exons, while no such accumulation was found on other exons (Figure S1D). This result suggests that RNAPII pauses near exons that are positively affected by methylation, pointing to RNAPII pausing as a possible mechanism for the positive effect of DNA methylation on splicing, supporting other mechanisms of action through the kinetic model such as the case with CTCF (Shukla et al., 2011) and MeCP2 (Maunakea et al., 2013).

HP1β and DNA Methylation Work in Concert to Regulate Splicing Decisions

To this point, we have shown that DNA methylation's effect on splicing can be bi-directional—it can enhance or suppress inclusion level of alternative exons. Previous studies have uncovered two mechanisms for methylation-dependent regulation of splicing (Maunakea et al., 2013; Shukla et al., 2011). However, these two mechanisms combined can only explain a small fraction of the overall regulatory effect of DNA methylation on splicing. Our search for other candidates that can directly affect splicing through DNA methylation has led us to HP1 proteins. As detailed above, previous evidence links HP1 to splicing regulation in some specific contexts, while other evidence links HP1 to H3K9me3, a heterochromatin-associated histone modification that can be co-localized with regions of methylated DNA. Combining this evidence makes HP1 a promising candidate to connect DNA methylation and splicing. To extend our observations on DNA methylation and to test the contribution of HP1 proteins on splicing in a genome-wide manner, we performed RNA-seq experiments on wild-type mouse ESCs, after knocking down each and all three HP1 isoforms (Figure 2A). RNA-seq experiments showed that there is a strong overlap among the three HP1 isoforms in the groups of affected exons, which encompasses approximately 70%–80% of the affected exons (Figure S2). This means that exons that were affected in a specific manner (positive or negative) by one isoform were usually affected in the same manner by the other two isoforms. Interestingly, this result suggests that the function of regulating alternative splicing is not limited to any single HP1 isoform. In fact, all three HP1 proteins probably share similar modes of action for alternative splicing regulation. This strong overlap in effects of all HP1 isoforms enabled us to take HP1β as a sole representative of this protein family and examine its effects on splicing. Of 2,837 alternative exons that met our strict criteria, 1,266 (44.6%) exons changed their inclusion levels by more than 10% when HP1β was knocked down (Figure 2B). Of these, 950 (33.5%) decreased their inclusion level and thus were positively affected by HP1β, and 316 (11.1%) increased their inclusion level and thus were negatively affected by HP1β. These results indicate that HP1β (as also HP1α and HP1γ), akin to DNA methylation itself, can influence alternative splicing in both directions, having both positive (enhancing) and negative (silencing) roles in exon recognition. We found that exons positively affected by HP1β are very long, as are exons positively affected by DNA methylation, while negatively affected exons are short (Figure 2C).

To examine whether splicing regulation by DNA methylation is related to HP1's effect, we looked for the exons that are affected in the same manner (either positively or negatively) by both DNA methylation and HP1. The results present an overlap between exons affected similarly by DNA methylation and HP1β that is highly significant compared to a random distribution (Figures 2D and 2E; proportions test, p value $< 2.2 \times 10^{-16}$; see Supplemental Experimental Procedures). This points to a strong correlation between the mechanisms of action involving DNA methylation and HP1β, as 152 exons, corresponding to 20%

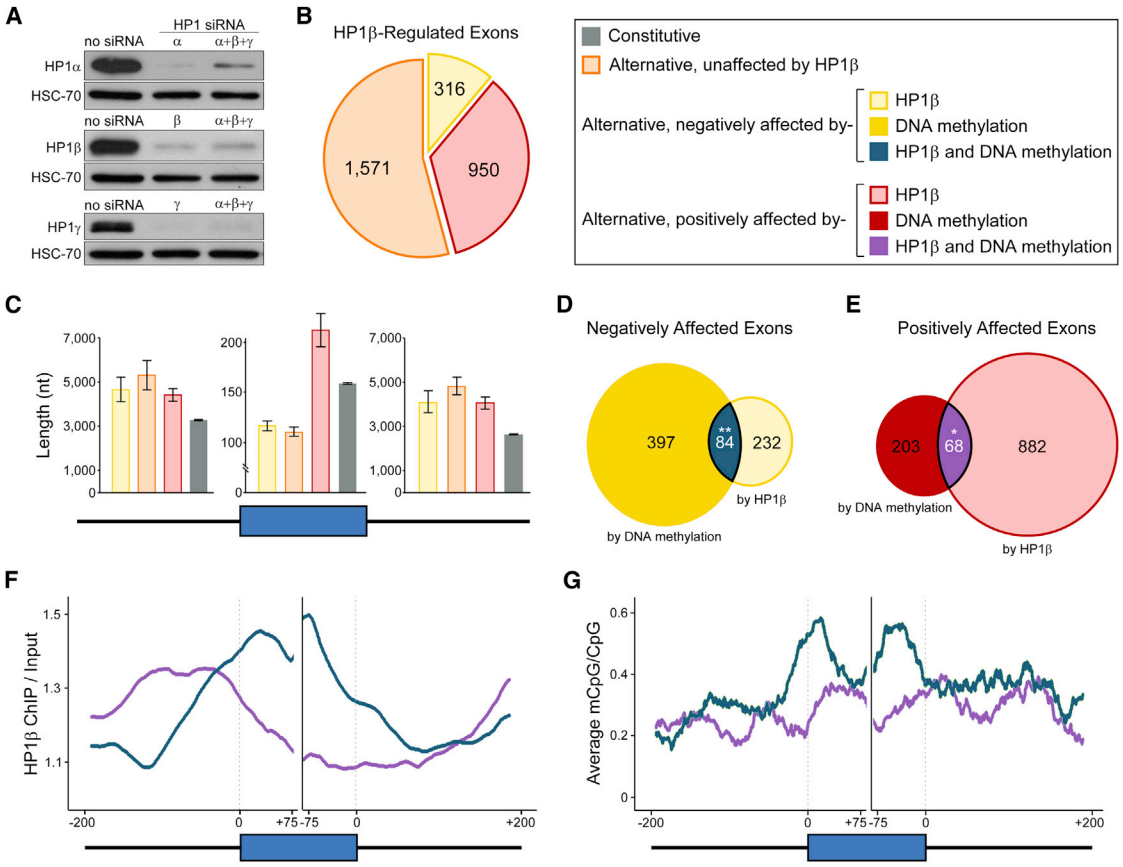

Figure 2. Identification and Characterization of HP1β- and DNA Methylation-Dependent Exons

(A) Western blot analysis of protein extracts from R1 wild-type cells treated with indicated siRNAs. HSC-70 was used as loading control.

(B) Distribution of alternative exons based on direction of change in splicing pattern between R1 cells treated with HP1β siRNA and untreated cells.

(C) Average length of upstream introns (left), exons (center), and downstream introns (right) for alternative (three groups) and constitutive exons.

(D) Overlap of exons that were negatively affected by DNA methylation and HP1β.

(E) Overlap of exons that were positively affected by DNA methylation and HP1β.

(F) Normalized HP1β ChIP-seq read signal of negatively (dark green) and positively (purple) affected overlapping exons based on (C) and (D).

(G) Average of methylated CpGs of negatively (dark green) and positively (purple) affected overlapping exons.

*Proportions test, $p < 1.3 \times 10^{-14}$; **proportions test, $p < 2.2 \times 10^{-16}$. See also Figure S2.

(152/752; Figures 2D and 2E) of the methylation-affected exons, can be explained by HP1 regulation. To study the biological function of the combined effects of DNA methylation and HP1, we performed Gene Ontology analysis using the DAVID tool (Huang da et al., 2009). Exons that are downregulated by both HP1 and methylation show strong enrichment for genes that take part in cell differentiation processes (p value = 0.005). This finding is of strong value, since the high methylation levels found in this group are a strong property of ESCs (Lister et al., 2009), where regulation of genes involved in differentiation is of major consequence. Indeed, when we attempt to differentiate the TKO cells by retinoic acid treatment, the cells die after 5 days of treatment, achieving only partial differentiation. This observation fits well, as misregulation of genes important for cell differentiation can lead to abnormal differentiation and subsequently to cell death. On the other hand, exons that are upregulated by both factors are enriched in genes that take part in translation regulation (p value = 0.002) and can play a role in regulating gene expression in different tissues and multiple developmental stages.

To examine HP1β binding profiles in the two exon groups (exons that are up- or downregulated by both HP1 and DNA methylation), we analyzed recently published HP1β ChIP-seq data of wild-type mouse ESCs (Müller-Ott et al., 2014). Remarkably, alternative exons that were negatively regulated by both methylation and HP1β showed a significant HP1β signal within the exon itself (t test, p value $< 2.2 \times 10^{-16}$), whereas exons that were positively regulated by both methylation and HP1β showed HP1β enrichment in the upstream intron (Figure 2F). We also examined DNA methylation patterns on these exons. Consistently with the HP1β signal, we found strong methylation signals at both ends of the negatively affected exons (Figure 2G), while the positive effect was consistently accompanied by low methylation levels (see Figure 1B). These results strongly suggest that HP1β, a DNA binding protein, can affect RNA alternative splicing in a context-dependent manner: it acts as a splicing

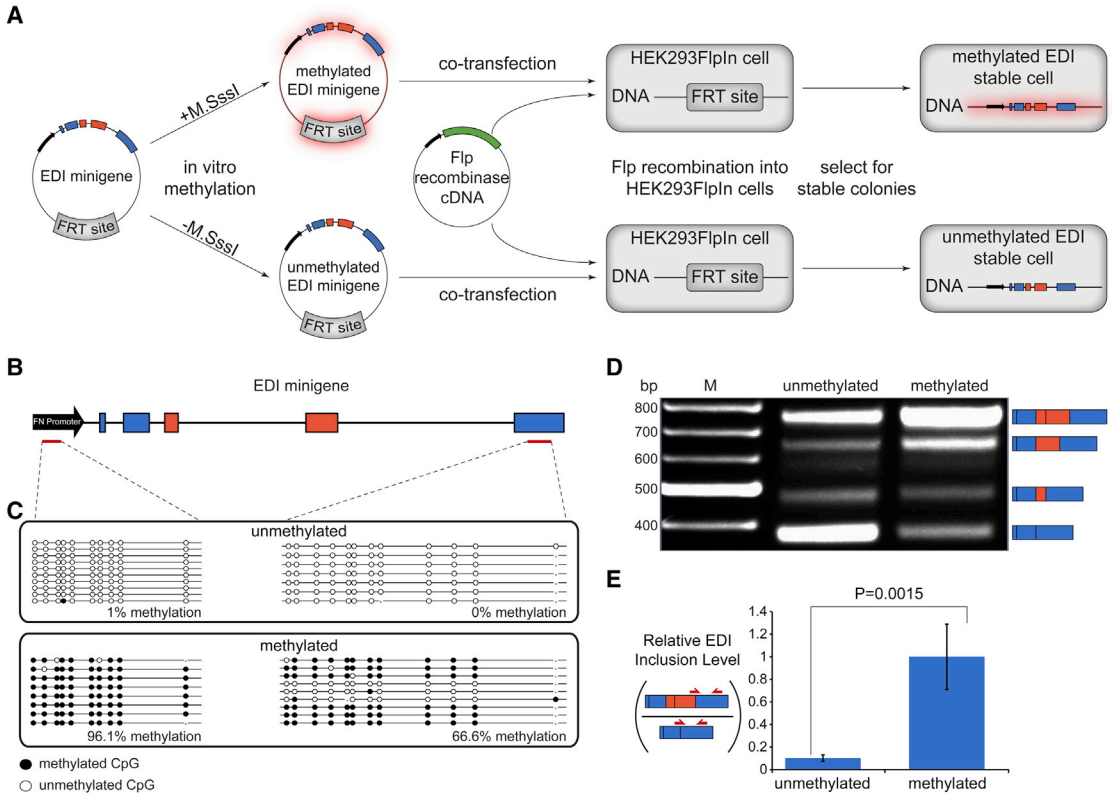

Figure 3. DNA Methylation Directly Affects Alternative Splicing

(A) Diagram illustrating the construction of the methylated and unmethylated EDI minigene experimental system.

(B) Schematic diagram of the EDI minigene. Constitutive and alternative exons are shown in blue and orange, respectively.

(C) Bisulfate sequencing of two representative regions (in red) on genomic DNA from cells containing unmethylated and methylated EDI. Below each plot is the methylation percentage of each region.

(D) RT-PCR of RNA from cells containing unmethylated and methylated EDI. The upper and lower bands represent inclusion and skipping of alternative exons, respectively.

(E) qRT-PCR of RNA from cells containing unmethylated and methylated EDI. Exon-exon junction primers for each isoform are represented by red arrows. EDI inclusion level was calculated by dividing amount of the inclusion isoform by amount of the skipping isoform. Values represent the mean ± SEM (n = 4). Student's t test was used to compare the indicated samples. See also Figure S3.

silencer when bound to a methylated exon and as a splicing enhancer when it binds immediately upstream to long exons.

Targeted Methylation of a Single Gene Supports a Direct Methylation Effect on mRNA Splicing

Thus far, we have shown that DNA methylation can affect exon splicing bi-directionally. We next aimed to validate our genome-wide results in an isolated and carefully controlled system. To establish a causative connection between the factors at hand, we constructed an experimental system in which differential DNA methylation could be limited to a single gene while all other cellular factors remain identical. For that purpose, we constructed a novel biological system that takes advantage of the fibronectin EDI minigene. This minigene system offers a well-established model system that has been used extensively in the past to study splicing regulatory mechanisms (Iannone and Valcárcel, 2013). We introduced this minigene, either in vitro CpG methylated or unmethylated (see Supplemental Experimental Procedures), into human Flp-In-HEK293 cells using targeted Flp recombination (Figures 3A and 3B). This system offers three advantages. First, the system enabled us to evaluate the effect of DNA methylation on one gene while the rest of the genome was unperturbed. Second, the gene was integrated into the genome and was thus studied in a normal genomic context. Third, methylated and unmethylated versions were introduced in the same orientation into the same genomic location, thus eliminating any confounding positional or other background effects. Following genomic insertion, we confirmed the methylation state using bisulfite sequencing for two representative regions and found that unmethylated EDI remained unmethylated, while methylated EDI remained mostly methylated after integration into the cells (Figure 3C). We next examined the splicing pattern of methylated versus unmethylated EDI exons using RT-PCR and qRT-PCR. Inclusion levels of the alternatively spliced exons were significantly higher in cells containing the methylated EDI gene than in cells containing the unmethylated EDI gene (Figures 3D and 3E). The endogenous EDI exon also displays a similar pattern, where high levels of DNA methylation coincide with high exon inclusion (Figure S3). Our genome-wide results indicate that DNA methylation can act as a splicing enhancer on

certain exons and as a splicing silencer on another fraction of exons (Figure 1A). The EDI minigene represents an example for a splicing enhancing ability. This effect is strongly supported by the genome-wide analysis (see Figure 1) when considering the similar structural features of the two EDI alternative exons and the generally affected exon population; both EDI exons display a high G+C content signal on the exon sequence and the sequence downstream of the 5′ splice site. Additionally, the second alternative exon is very long (270 nt), and both exons have a stronger 3′ splice site. Most importantly, this result provides for the first time a direct and causal link between DNA methylation and splicing. It indicates that DNA methylation, specifically on the EDI minigene, is directly involved in splicing regulation of its alternative exons. This result is accentuated by the fact that both cell types, harboring either a methylated or an unmethylated EDI minigene, share identical genomic and epigenomic backgrounds.

HP1 Mediates DNA Methylation and Splicing

Our genome-wide results indicate that HP1 proteins can regulate alternative splicing bi-directionally, explaining a substantial portion of DNA methylation's global effect on splicing. We next used our EDI experimental system to validate these genome-wide results regarding HP1's part in this mechanism. To test if HP1 serves as a mediator connecting DNA methylation with splicing, we first examined the role of HP1 proteins in our system by overexpressing or knocking down each of the three HP1 isoforms (Figure S4A). In the case of an unmethylated EDI, both overexpression and knockdown of all HP1 isoforms caused a general slight decrease in EDI inclusion levels (Figures S4B and S4C). In contrast, when EDI is methylated, HP1 manipulation gave a differential effect: overexpression of HP1 caused a prominent decrease in EDI inclusion (Figure S4B), while knockdown of HP1 caused an increase in EDI inclusion levels (Figure S4C). Given that the splicing effect on unmethylated EDI was similar for both overexpression and knockdown of all HP1 isoforms, we regard this as a background effect, which is probably indirect. To normalize this background, we divided the effect of changed HP1 levels on methylated EDI by the respective effect of changed HP1 levels on unmethylated EDI. Knockdown of HP1α and HP1β isoforms caused a stronger shift toward higher inclusion for a methylated EDI minigene, whereas overexpression of these isoforms produced the opposite effect (Figure 4A). Notably, changes in levels of HP1γ did not significantly affect the methylation-induced shift in splicing patterns. These results suggest that HP1α and HP1β suppress EDI exon recognition in a methylation-dependent manner. Our genome-wide results indicate that HP1 can act as a splicing enhancer on a certain group of exons and as a splicing silencer for a different group of exons (Figure 2B). In this system, we observe an example for its ability to interfere with exon recognition when the exon is methylated. Here, we find that DNA methylation's "natural" effect is to enhance exon recognition. However, methylation-dependent binding of HP1α and HP1β to the minigene disrupts EDI exon recognition. DNA methylation can regulate splicing through multiple factors in addition to HP1, both known (Maunakea et al., 2013; Shukla et al., 2011) and unknown. Here, we observe a possible competition between factors, meaning that the binding of other methyl binding regulatory proteins might exert a regulatory effect on EDI alternative splicing that is in competition with HP1.

To search for the mechanism by which this methylation-dependent regulation by HP1 occurs, we first investigated how HP1 proteins bind to the EDI gene using ChIP-qPCR. Importantly, we found significant enrichment of all three HP1 isoforms across the methylated, but not the unmethylated, EDI gene, indicating their expected association with methylated DNA. Furthermore, all HP1 proteins show specific binding peaks on the two methylated alternative exons and in the promoter region (Figure 4B). This result is fully consistent with our genome-wide observations, showing that HP1 silenced exon recognition when it bound to the alternative exon itself (Figure 2F).

It was previously shown that H3K9me3 functions as a substrate for HP1's binding to chromatin (Bannister et al., 2001; Jacobs and Khorasanizadeh, 2002). We therefore used ChIP-qPCR analysis to examine where along the minigene H3K9me3 is located. We found enrichment patterns similar to that of HP1, i.e., a strong enrichment on the methylated, but not the unmethylated, EDI gene, with specific peaks on the alternative exons and the promoter region (Figure 4B). These results show high correlation between HP1 isoforms and H3K9me3 along the minigene, specifically when alternative exons are affected. Comparing the signal of H3K9me3 to the nucleosome occupancy signal on the methylated EDI (Figure S4D; histone H3) allowed us to safely conclude that H3K9me3 is not a byproduct of increased nucleosome occupancy. Also, other histone marks such as H3K9me2 and H3K36me3 were largely unaffected by EDI methylation, supporting the expected result that indeed HP1 isoforms are associated via H3K9me3 (Figure S4D).

HP1 Recruits the Splicing Factor SRSF3

HP1 was previously shown to be associated with splicing factors SRSF1 in mitotic HeLa cells (Loomis et al., 2009), and heterogeneous nuclear ribonucleoprotein particles (hnRNPs) in *Drosophila* and humans (Ameyar-Zazoua et al., 2012; Piacentini et al., 2009). To examine whether this interaction occurs in our system, we performed co-immunoprecipitation assays to probe for the interaction of HP1 proteins with various splicing factors, which we suspected could associate with HP1. Of the examined splicing factors, we found that SF3B1, SRSF1, and SRSF3 bind to HP1α and HP1β isoforms, but not to HP1γ (Figure 4C). This interaction was not sensitive to RNase treatment (see Experimental Procedures). We did not find HP1 to associate with other splicing factors such as SRSF6 and hnRNP A2/B1. We also did not detect any association between HP1 isoforms and RNAPII (Figure 4C), although this interaction was previously reported in *Drosophila* (Piacentini et al., 2009). Our finding that HP1 associates with SF3B1, a U2 small nuclear ribonucleoprotein particle (snRNP)-associated protein, led us to examine whether the whole U2 snRNP associates with HP1. Further co-immunoprecipitation experiments showed that all other tested U2 snRNP components also associated with HP1 (Figure S4E), which suggests that the whole U2 snRNP could be associated with HP1 and that HP1 might help recruit U2 snRNP to H3K9 methylated histones, similarly to CHD1's known recruitment of U2 snRNP to H3K4 methylated histones (Sims et al., 2007). Overall, the

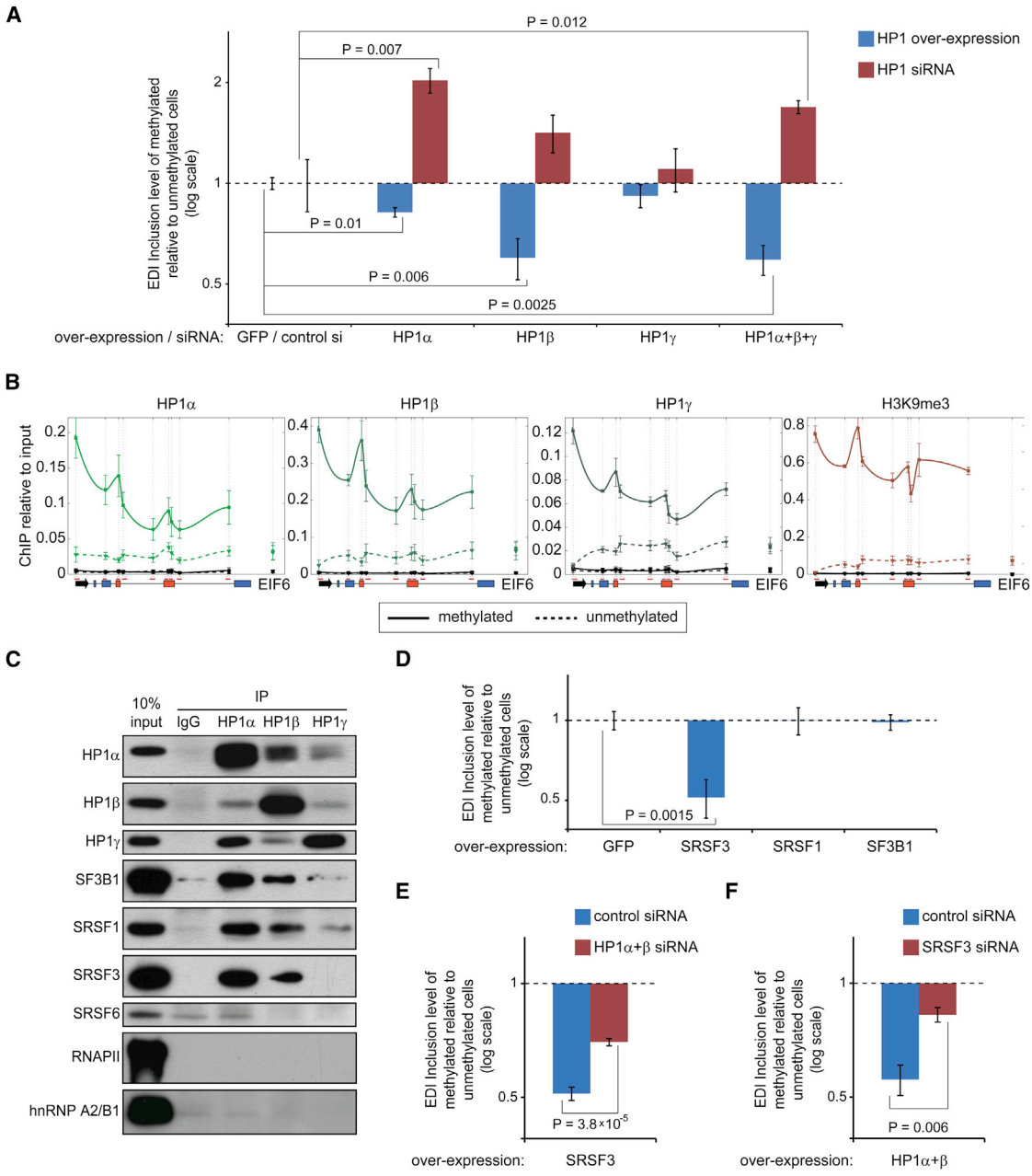

Figure 4. HP1 Mediates Splicing Changes in a Methylation-Dependent Manner by Recruiting SRSF3

(A) HP1 was overexpressed or knocked down using siRNA in methylated and unmethylated cells, and qRT-PCR analysis using the previously indicated exon-exon junction primers was used to assess EDI inclusion level of methylated relative to unmethylated cells (n = 3).

(B) ChIP of HP1 isoforms and H3K9me3 in unmethylated and methylated cells and qPCR along the EDI minigene using EIF6 intron 3 for endogenous background control. Values are ChIP relative to input (n = 3). Dotted and full lines represent the ChIP signal in unmethylated and methylated cells, respectively. Black lines represent ChIP with rabbit IgG.

(C) Co-immunoprecipitation of HP1 isoforms with various splicing factors and RNA polymerase II (RNAPII) in Flp-In-HEK293 cells.

(D) Indicated splicing factors were overexpressed, and qRT-PCR analysis was used to assess EDI inclusion level of methylated relative to unmethylated cells (n = 5).

(E) SRSF3 was overexpressed and cells were treated with HP1 siRNA (red) or control siRNA (blue; n = 5). EDI inclusion levels of methylated relative to unmethylated cells were determined.

(F) HP1α and HP1β were overexpressed, and cells were treated with SRSF3 siRNA (red) or control siRNA (blue; n = 3). EDI inclusion levels of methylated relative to unmethylated cells were determined.

All graphs show mean values ± SEM. Student's t test was used to compare the indicated samples. See also Figures S4 and S5.

association of HP1 with splicing factors could mean that HP1's regulation of alternative splicing involves the recruitment of splicing factors to methylated DNA.

Thus far, we found that HP1α and HP1β, but not HP1γ, regulate EDI alternative splicing in a methylation-dependent manner (Figure 4A) and directly bind to splicing factors (Figure 4C). To further study the underlying mechanism, we tested whether HP1 functions as an adaptor protein that recognizes H3K9me3 and recruits splicing factors to the EDI alternative exons. We overexpressed the HP1-bound splicing factors SF3B1, SRSF1, and SRSF3 in cells in which EDI was either methylated or unmethylated. Overexpression of SRSF1 or SF3B1 did not change the basic positive shift in EDI inclusion that accompanies methylation and is observed in the GFP control, whereas overexpression of SRSF3 reduced the positive splicing shift caused by DNA methylation (Figure 4D); this same result was observed previously when overexpressing HP1α or HP1β (Figure 4A), which suggests that HP1 might be responsible for recruiting SRSF3 to the methylated EDI gene. SRSF3's role as a splicing silencer in the EDI system was previously described (de la Mata and Kornblihtt, 2006). Therefore, overexpressing SRSF3 is expected to lower EDI alternative exon inclusion levels regardless of the methylation state. A deeper examination of the data shows that this is indeed the case; SRSF3 overexpression decreases EDI inclusion in both methylated and unmethylated states, but the magnitude of the effect differs significantly. After overexpressing SRSF3, inclusion of the EDI alternative exons shows a 6-fold drop when the gene is methylated but only a 3-fold drop when the gene is unmethylated (Figure S5A; Student's t test, p value = 0.0034). The stronger effect of SRSF3 on a methylated EDI can be explained by additional recruitment of SRSF3 through HP1 only in a methylated state. To confirm this hypothesis, we overexpressed SRSF3 while simultaneously knocking down HP1α and HP1β. Indeed, in the absence of HP1α and HP1β, overexpression of SRSF3 produced a significantly diminished effect on EDI splicing (Figure 4E). The diminished SRSF3 effect was limited only to the methylated EDI (Figures S5B and S5C) and was not a result of differences in SRSF3 transfection levels (Figure S5D). We also performed the reciprocal experiment, where we overexpressed HP1α and HP1β while simultaneously knocking down SRSF3. The results further strengthen this hypothesis, as in the absence of SRSF3, overexpression of HP1 produced a significantly diminished effect on EDI splicing (Figure 4F), which suggests that SRSF3 is required for HP1's methylation-dependent effect on splicing. Put together, these findings strongly support a methylation-dependent effect of SRSF3 on the EDI alternative exons that is mediated by HP1α and HP1β.

Overall, we present here a mechanism that encompasses both DNA and RNA levels and is controlled epigenetically: methylated EDI alternative exons are enriched with the H3K9me3 modification, which acts as the substrate for HP1 proteins. HP1 proteins are therefore found particularly on the methylated EDI alternative exons. The strong association of HP1α and HP1β with SRSF3 enhances SRSF3's role as a splicing silencer in this system, lowering the inclusion levels of the EDI alternative exons, and creates the final link between DNA methylation, HP1, and splicing regulation.

DISCUSSION

The question regarding the impact of DNA methylation on the splicing process has been raised numerous times in recent years, yet knowledge about DNA methylation's regulatory effect remains limited and incomplete. Here, we use a genome-wide approach to discern DNA methylation's global ability to regulate alternative splicing. The various deep-sequencing experiments that we performed on methylation-deficient cells highlight the significant global impact that DNA methylation has on alternative splicing, both positive and negative. Altered DNA methylation levels affect the splicing of more than one-fifth of alternative exons, showing a surprisingly extensive range of influence. In contrast, DNA methylation did not have a profound effect on constitutively spliced exons, as almost all constitutive exons in wild-type cells remain so in TKO cells. We therefore suspect that DNA methylation is more of a "fine-tuning" mechanism and is unable to overcome the strong splicing signals inherent in constitutive exons. Taking into account DNA methylation's significant influence on splicing of alternative exons, this epigenetic modification will have a major contribution to current splicing prediction tools such as the "splicing code" (Barash et al., 2010), and we strongly support its introduction to these tools.

The finding that constitutive exons exhibit higher methylation levels than alternative exons implies that DNA methylation promotes exon inclusion. However, we propose that DNA methylation's fine-tuned regulation of splicing is only made apparent in alternative exons whose recognition, unlike constitutive exons, is not strongly controlled by the basic splicing recognition factors. When analyzing alternative exons that are affected or unaffected by methylation, we find that the underlying mechanism is indeed more complex: high methylation levels will repress recognition of alternative exons, while low methylation levels will enhance their recognition. We hypothesize that constitutive exons might have high inclusion in spite of and not because of high DNA methylation levels, as these exons are controlled by much stronger intrinsic factors that overshadow DNA methylation's weaker effects.

The search for a mediator protein that can affect splicing regulation on the one hand and is selective to DNA methylation on the other led us to examine the HP1 protein family. Our global analysis of the HP1 proteins points to significant similarities between HP1 and DNA methylation regarding their effect on alternative splicing. Quite strikingly, our combined genome-wide results demonstrate that for 152 alternative exons, which represent 20% of the overall effect of DNA methylation on splicing, splicing regulation can be explained by an interaction with HP1. This correlation is highly significant compared to random chance. The number of exons that are affected here is not large, but it reflects other mechanisms of refined splicing regulation by DNA binding proteins such as those published by a landmark study done by Luco et al. showing that 65 exons, which correspond to 14% of PTB-regulated exons, could be explained by regulation through MRG15 (Luco et al., 2010). In addition to DNA methylation, there might be other potential mechanisms for HP1-mediated alternative splicing, as HP1 was previously shown to bind to RNA (Muchardt et al., 2002). The existence of other, methylation-independent mechanisms could explain the non-overlapping

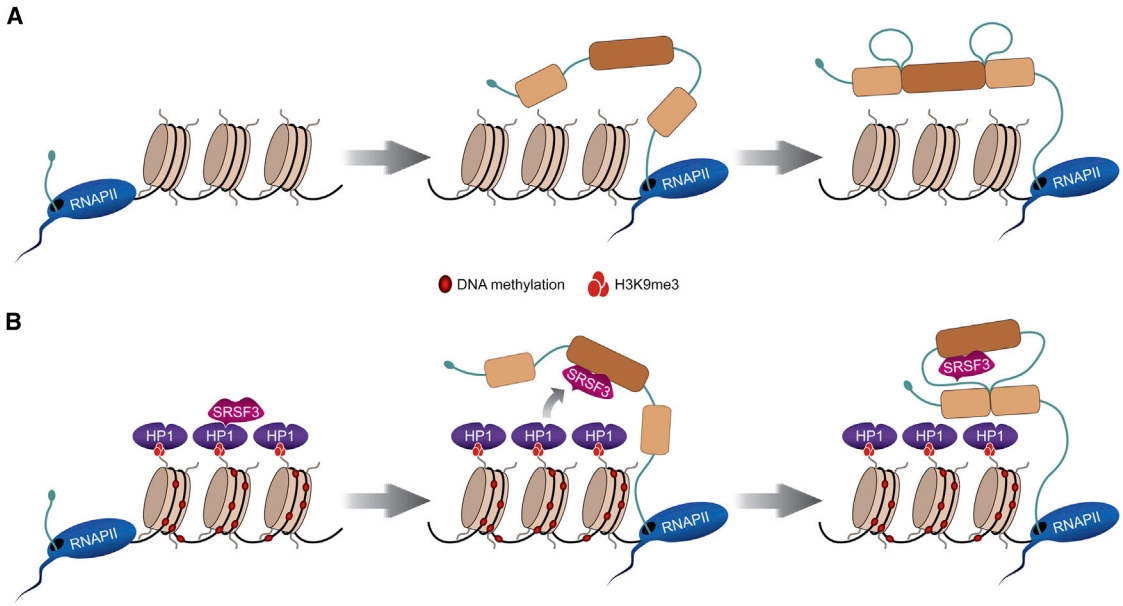

Figure 5. A Model for How HP1 Links DNA Methylation to Alternative Splicing in the EDI System

(A) When DNA is unmethylated, RNAPII (blue) transcribes the pre-mRNA molecule and the EDI alternative exon (dark brown) is included in the mature transcript. (B) When DNA is methylated (dark red circle), the histone modification H3K9me3 (three red circles) is present and HP1 (purple) binds to the chromatin. The splicing factor SRSF3 (pink) binds to HP1 and is transferred to the pre-mRNA, resulting in skipping of the EDI alternative exon in the mature transcript.

alternative splicing events. Overall, our results suggest that HP1 serves an important function as a mediator between DNA methylation and splicing, thus adding another layer of regulation to other known mechanisms of splicing regulation through DNA methylation such as CTCF (Shukla et al., 2011) and MeCP2 (Maunakea et al., 2013). Remarkably, our ChIP-seq results demonstrate a localization specific effect for HP1 on RNA splicing (Figure 2F): HP1 enhances the inclusion of exons when bound immediately upstream to the exon and silences exon recognition when bound to the exon itself. This position-specific effect has been observed before for multiple RNA binding proteins such as PTB (Llorian et al., 2010) and hnRNP proteins (Huelga et al., 2012) and is shown here for the first time for a DNA binding protein.

A strong backup to our genome-wide analysis was performed using a newly introduced system that uses site-specific targeting of a methylated gene versus an unmethylated gene. This system produced two major discoveries.

First, the overwhelming majority of papers dealing with regulation of alternative splicing by DNA methylation make use of correlational observations. Consequently, the major question in the field—whether there is a direct link between methylation and splicing—remained unanswered. Here, using our EDI experimental system, we were able to switch on or switch off DNA methylation in a single gene while keeping the endogenous background unchanged. This enormous advantage allowed us to overcome that common limitation and demonstrate for the first time a causal relationship between DNA methylation and alternative splicing.

Second, using our EDI experimental system, we show that HP1 is an adaptor protein that connects DNA methylation to splicing by recruiting splicing factors. We found that HP1α and HP1β bind to methylated EDI alternative exons and recruit the splicing factor SRSF3, thus enhancing SRSF3's role as a splicing silencer in this system and lowering the inclusion levels of the EDI alternative exons in their methylated state. DNA methylation has been shown previously to regulate splicing through an impact on the kinetics of RNAPII elongation (Maunakea et al., 2013). However, the mechanism presented here represents the first reported example of DNA methylation's ability to regulate alternative splicing through the recruitment model. We therefore propose a model by which HP1 binds to the DNA methylation-associated histone modification H3K9me3 and recruits splicing factors specifically to methylated alternative exons (Figure 5). This recruitment reduces exon recognition in the EDI system, where HP1 binds to the EDI alternative exons. HP1 can also enhance exon recognition in other cases, where it binds upstream to the alternative exons, as our results show a localization-specific effect for HP1 on splicing (Figure 2F).

Our RNA-seq experiments show that all three HP1 isoforms can regulate alternative splicing. Moreover, our results display a high level of overlap (70%–80%) between the exon populations that were affected by the different HP1 proteins (Figure S2), suggesting that the HP1 isoforms probably share similar modes of action. However, while this overlap is high, it is not complete, leaving the possibility for specific cases where HP1 proteins only partially overlap. The EDI system represents such a case, as both HP1α and HP1β affect alternative splicing similarly, whereas HP1γ does not strongly affect alternative splicing in this system.

The involvement of HP1 in the regulation of splicing by DNA methylation may be especially relevant in pathological

conditions, such as cancer, where widespread changes in levels of DNA methylation and aberrant alternative splicing patterns have been reported (David and Manley, 2010; Hodges et al., 2009), while overexpression of HP1 has also been detected in multiple cancer cell lines and is thought to play a role in tumorigenesis (Takanashi et al., 2009). Indeed, we found several known cases where alternative exons similarly regulated by both DNA methylation and HP1 are involved in cancer: the *Mnk* splicing isoform that includes exon 13 was found to be tumor suppressive and is downregulated in breast, lung, and colon tumors (Maimon et al., 2014); exon 12 of the *Irak1* gene affects its ability to phosphorylate and activate the NF-κB pathway (Carpenter et al., 2014) and is an oncotarget in both myelodysplastic syndromes and acute myeloid leukemia cancers (Beverly and Starczynowski, 2014; Rhyasen et al., 2013); and exon 6 of the *Myl6* gene and exon 8 of the *App* gene were found to have differential splicing patterns in breast cancer and lung cancer, respectively (Li et al., 2006; Misquitta-Ali et al., 2011). These examples highlight the importance of HP1-mediated regulation of splicing by DNA methylation on cancer progression.

Finally, it is likely that additional methylation-dependent splicing regulatory proteins exist, and the novel model system that we present here offers the scientific community a unique opportunity to probe and discover such proteins in the future.

EXPERIMENTAL PROCEDURES

Detailed experimental procedures can be found in Supplemental Experimental Procedures.

Cells and Plasmids

Flp-In-HEK293 cells were from Invitrogen. Mouse R1 ESCs were from ATCC. Dnmt TKO ESCs were a kind gift from Prof. Masaki Okano (RIKEN) and have been previously described previously (Tsumura et al., 2006). The expression plasmids encoding HP1α-GFP, HP1β-GFP, HP1γ-GFP, SRSF1-T7, and SRSF3-T7 were previously described (Cáceres et al., 1997; Cheutin et al., 2003). The expression plasmid encoding the SF3B1-GFP fusion protein was a kind gift from Prof. Juan Valcarcel (Centre de Regulació Genòmica). pSVEDA/FN containing the EDI minigene was a kind gift from Prof. Alberto Kornblihtt (Universidad de Buenos Aires) and has been previously described (Cramer et al., 1999). The EDI minigene was introduced into pcDNA5/FRT/TO (Invitrogen) for stable integration into the cells.

EDI Bisulfite Sequencing

DNA was extracted from cells, bisulfite converted, and PCR amplified. The PCR product was cloned into a plasmid and transformed into bacteria. DNA from several colonies was extracted and sequenced using the forward primer from the PCR reaction.

Analysis of Splicing Patterns by RT-PCR and qRT-PCR

Total RNA was reverse transcribed using SuperScript III (Invitrogen). For RT-PCR analysis, PCR was performed using Biotools DNA Polymerase, and resulting products were visualized on agarose gels. For qRT-PCR, qPCR was performed using KAPA SYBR FAST on a Stratagene Mx3005P thermocycler using exon-exon junction primer pairs designed to detect the inclusion or skipping isoforms.

Overexpression and siRNA Knockdown

Expression plasmids were transfected using TransIT-LT1 (Mirus), and cells were incubated for 48 hr before RNA and proteins were extracted. In all experiments, an empty pEGFP-C3 plasmid was used for control. Knockdowns were performed using siGENOME small interfering RNAs (siRNAs) (Dharmacon). Stable cells were transfected using Lipofectamine RNAiMAX (Invitrogen) and incubated for 96 hr before RNA and proteins were extracted. R1 and TKO cells were transfected using Lipofectamine 2000 (Invitrogen) and incubated for 48 hr before RNA and proteins were extracted.

Co-immunoprecipitation

Cells were washed with PBS, and nuclei were purified and treated with MNase to release chromatin-bound proteins, then re-suspended in immunoprecipitation (IP) buffer and incubated with antibody conjugated to protein A Dynabeads (Invitrogen). Samples were incubated with RNase A and washed with IP buffer. Proteins were eluted and subjected to western blot analysis.

ChIP

Cells were cross-linked using formaldehyde, lysed, and sonicated to obtain an average DNA size of 150–350 bp. Chromatin was incubated with antibody conjugated to protein A Dynabeads (Invitrogen). Samples were stringently washed using several buffers. DNA was eluted, treated with RNase A and Proteinase K, and incubated at 65°C to reverse the cross-links. DNA was purified using MinElute PCR purification kit (QIAGEN) followed by qPCR analysis.

Library Preparation and Deep Sequencing

RNA-seq library preparation was performed using commercially available kits from Illumina. Deep sequencing was carried out on an Illumina Genome Analyzer II or Illumina HiSeq 2000.

ACCESSION NUMBERS

The GEO accession number for the sequence data reported in this paper is GSE64910.

SUPPLEMENTAL INFORMATION

Supplemental Information includes Supplemental Experimental Procedures, five figures, and two tables and can be found with this article online at http://dx.doi.org/10.1016/j.celrep.2015.01.038.

AUTHOR CONTRIBUTIONS

A.Y. designed and carried out all experiments following consultations with G.A. and E.M.; R.S. performed EDI bisulfite sequencing and HP1 overexpressions and knockdowns and helped with the creation of stable cells; S.M. maintained the mouse embryonic stem cells; S.G. performed all computational analyses with help from O.G.; A.Y. and S.G. wrote the manuscript; and A.Y., S.G., R.S., G.A., and E.M. discussed the results and commented on the manuscript.

ACKNOWLEDGMENTS

We thank Drs. Schraga Schwartz, Oren Ram, Ze'ev Melamed, and Dror Hollander for comments and critical reading of the manuscript. We thank Dr. Rani Elkon for statistical advice. G.A. was funded by grants from the Israel Science Foundation (ISF-Bikura 838/10, ISF 61/09), and from the Israel Cancer Research Foundation (ICRF PG-14/195). E.M. was supported by the Israel Science Foundation FIRST individual grant (ISF 1430/13), the Israel Science Foundation (ISF 1252/12, 657/12), the Abisch-Frenkel Foundation, an Israel-Germany MOST-DKFZ collaboration grant (with K.R.), and a European Research Council FP7 grant (ERC-281781). The funders had no role in study design, data collection and analysis, decision to publish, or preparation of the manuscript.

Received: August 12, 2014
Revised: December 3, 2014
Accepted: January 15, 2015
Published: February 19, 2015

REFERENCES

Alló, M., Buggiano, V., Fededa, J.P., Petrillo, E., Schor, I., de la Mata, M., Agirre, E., Plass, M., Eyras, E., Elela, S.A., et al. (2009). Control of alternative

Please cite this article in press as: Yearim et al., HP1 Is Involved in Regulating the Global Impact of DNA Methylation on Alternative Splicing, Cell Reports (2015), http://dx.doi.org/10.1016/j.celrep.2015.01.038

splicing through siRNA-mediated transcriptional gene silencing. Nat. Struct. Mol. Biol. *16*, 717–724.

Ameyar-Zazoua, M., Rachez, C., Souidi, M., Robin, P., Fritsch, L., Young, R., Morozova, N., Fenouil, R., Descostes, N., Andrau, J.C., et al. (2012). Argonaute proteins couple chromatin silencing to alternative splicing. Nat. Struct. Mol. Biol. *19*, 998–1004.

Amit, M., Donyo, M., Hollander, D., Goren, A., Kim, E., Gelfman, S., Lev-Maor, G., Burstein, D., Schwartz, S., Postolsky, B., et al. (2012). Differential GC content between exons and introns establishes distinct strategies of splice-site recognition. Cell Rep. *1*, 543–556.

Ball, M.P., Li, J.B., Gao, Y., Lee, J.H., LeProust, E.M., Park, I.H., Xie, B., Daley, G.Q., and Church, G.M. (2009). Targeted and genome-scale strategies reveal gene-body methylation signatures in human cells. Nat. Biotechnol. *27*, 361–368.

Bannister, A.J., Zegerman, P., Partridge, J.F., Miska, E.A., Thomas, J.O., Allshire, R.C., and Kouzarides, T. (2001). Selective recognition of methylated lysine 9 on histone H3 by the HP1 chromo domain. Nature *410*, 120–124.

Barash, Y., Calarco, J.A., Gao, W., Pan, Q., Wang, X., Shai, O., Blencowe, B.J., and Frey, B.J. (2010). Deciphering the splicing code. Nature *465*, 53–59.

Beverly, L.J., and Starczynowski, D.T. (2014). IRAK1: oncotarget in MDS and AML. Oncotarget *5*, 1699–1700.

Cáceres, J.F., Misteli, T., Screaton, G.R., Spector, D.L., and Krainer, A.R. (1997). Role of the modular domains of SR proteins in subnuclear localization and alternative splicing specificity. J. Cell Biol. *138*, 225–238.

Carpenter, S., Ricci, E.P., Mercier, B.C., Moore, M.J., and Fitzgerald, K.A. (2014). Post-transcriptional regulation of gene expression in innate immunity. Nat. Rev. Immunol. *14*, 361–376.

Cheutin, T., McNairn, A.J., Jenuwein, T., Gilbert, D.M., Singh, P.B., and Misteli, T. (2003). Maintenance of stable heterochromatin domains by dynamic HP1 binding. Science *299*, 721–725.

Chodavarapu, R.K., Feng, S., Bernatavichute, Y.V., Chen, P.Y., Stroud, H., Yu, Y., Hetzel, J.A., Kuo, F., Kim, J., Cokus, S.J., et al. (2010). Relationship between nucleosome positioning and DNA methylation. Nature *466*, 388–392.

Cramer, P., Cáceres, J.F., Cazalla, D., Kadener, S., Muro, A.F., Baralle, F.E., and Kornblihtt, A.R. (1999). Coupling of transcription with alternative splicing: RNA pol II promoters modulate SF2/ASF and 9G8 effects on an exonic splicing enhancer. Mol. Cell *4*, 251–258.

David, C.J., and Manley, J.L. (2010). Alternative pre-mRNA splicing regulation in cancer: pathways and programs unhinged. Genes Dev. *24*, 2343–2364.

de la Mata, M., and Kornblihtt, A.R. (2006). RNA polymerase II C-terminal domain mediates regulation of alternative splicing by SRp20. Nat. Struct. Mol. Biol. *13*, 973–980.

Gelfman, S., Burstein, D., Penn, O., Savchenko, A., Amit, M., Schwartz, S., Pupko, T., and Ast, G. (2012). Changes in exon-intron structure during vertebrate evolution affect the splicing pattern of exons. Genome Res. *22*, 35–50.

Gelfman, S., Cohen, N., Yearim, A., and Ast, G. (2013). DNA-methylation effect on cotranscriptional splicing is dependent on GC architecture of the exon-intron structure. Genome Res. *23*, 789–799.

Hashimshony, T., Zhang, J., Keshet, I., Bustin, M., and Cedar, H. (2003). The role of DNA methylation in setting up chromatin structure during development. Nat. Genet. *34*, 187–192.

Heyn, H., Moran, S., Hernando-Herraez, I., Sayols, S., Gomez, A., Sandoval, J., Monk, D., Hata, K., Marques-Bonet, T., Wang, L., and Esteller, M. (2013). DNA methylation contributes to natural human variation. Genome Res. *23*, 1363–1372.

Hodges, E., Smith, A.D., Kendall, J., Xuan, Z., Ravi, K., Rooks, M., Zhang, M.Q., Ye, K., Bhattacharjee, A., Brizuela, L., et al. (2009). High definition profiling of mammalian DNA methylation by array capture and single molecule bisulfite sequencing. Genome Res. *19*, 1593–1605.

Huang da, W., Sherman, B.T., and Lempicki, R.A. (2009). Systematic and integrative analysis of large gene lists using DAVID bioinformatics resources. Nat. Protoc. *4*, 44–57.

Huelga, S.C., Vu, A.Q., Arnold, J.D., Liang, T.Y., Liu, P.P., Yan, B.Y., Donohue, J.P., Shiue, L., Hoon, S., Brenner, S., et al. (2012). Integrative genome-wide analysis reveals cooperative regulation of alternative splicing by hnRNP proteins. Cell Rep. *1*, 167–178.

Huff, J.T., and Zilberman, D. (2014). Dnmt1-independent CG methylation contributes to nucleosome positioning in diverse eukaryotes. Cell *156*, 1286–1297.

Iannone, C., and Valcárcel, J. (2013). Chromatin's thread to alternative splicing regulation. Chromosoma *122*, 465–474.

Jacobs, S.A., and Khorasanizadeh, S. (2002). Structure of HP1 chromodomain bound to a lysine 9-methylated histone H3 tail. Science *295*, 2080–2083.

Laurent, L., Wong, E., Li, G., Huynh, T., Tsirigos, A., Ong, C.T., Low, H.M., Kin Sung, K.W., Rigoutsos, I., Loring, J., and Wei, C.L. (2010). Dynamic changes in the human methylome during differentiation. Genome Res. *20*, 320–331.

Li, C., Kato, M., Shiue, L., Shively, J.E., Ares, M., Jr., and Lin, R.J. (2006). Cell type and culture condition-dependent alternative splicing in human breast cancer cells revealed by splicing-sensitive microarrays. Cancer Res. *66*, 1990–1999.

Lister, R., Pelizzola, M., Dowen, R.H., Hawkins, R.D., Hon, G., Tonti-Filippini, J., Nery, J.R., Lee, L., Ye, Z., Ngo, Q.M., et al. (2009). Human DNA methylomes at base resolution show widespread epigenomic differences. Nature *462*, 315–322.

Llorian, M., Schwartz, S., Clark, T.A., Hollander, D., Tan, L.Y., Spellman, R., Gordon, A., Schweitzer, A.C., de la Grange, P., Ast, G., and Smith, C.W. (2010). Position-dependent alternative splicing activity revealed by global profiling of alternative splicing events regulated by PTB. Nat. Struct. Mol. Biol. *17*, 1114–1123.

Loomis, R.J., Naoe, Y., Parker, J.B., Savic, V., Bozovsky, M.R., Macfarlan, T., Manley, J.L., and Chakravarti, D. (2009). Chromatin binding of SRp20 and ASF/SF2 and dissociation from mitotic chromosomes is modulated by histone H3 serine 10 phosphorylation. Mol. Cell *33*, 450–461.

Luco, R.F., Pan, Q., Tominaga, K., Blencowe, B.J., Pereira-Smith, O.M., and Misteli, T. (2010). Regulation of alternative splicing by histone modifications. Science *327*, 996–1000.

Lyko, F., Foret, S., Kucharski, R., Wolf, S., Falckenhayn, C., and Maleszka, R. (2010). The honey bee epigenomes: differential methylation of brain DNA in queens and workers. PLoS Biol. *8*, e1000506.

Maimon, A., Mogilevsky, M., Shilo, A., Golan-Gerstl, R., Obiedat, A., Ben-Hur, V., Lebenthal-Loinger, I., Stein, I., Reich, R., Beenstock, J., et al. (2014). Mnk2 alternative splicing modulates the p38-MAPK pathway and impacts Ras-induced transformation. Cell Rep. *7*, 501–513.

Maunakea, A.K., Chepelev, I., Cui, K., and Zhao, K. (2013). Intragenic DNA methylation modulates alternative splicing by recruiting MeCP2 to promote exon recognition. Cell Res. *23*, 1256–1269.

Melcer, S., Hezroni, H., Rand, E., Nissim-Rafinia, M., Skoultchi, A., Stewart, C.L., Bustin, M., and Meshorer, E. (2012). Histone modifications and lamin A regulate chromatin protein dynamics in early embryonic stem cell differentiation. Nat. Commun. *3*, 910.

Misquitta-Ali, C.M., Cheng, E., O'Hanlon, D., Liu, N., McGlade, C.J., Tsao, M.S., and Blencowe, B.J. (2011). Global profiling and molecular characterization of alternative splicing events misregulated in lung cancer. Mol. Cell. Biol. *31*, 138–150.

Muchardt, C., Guilleme, M., Seeler, J.S., Trouche, D., Dejean, A., and Yaniv, M. (2002). Coordinated methyl and RNA binding is required for heterochromatin localization of mammalian HP1alpha. EMBO Rep. *3*, 975–981.

Müller-Ott, K., Erdel, F., Matveeva, A., Mallm, J.P., Rademacher, A., Hahn, M., Bauer, C., Zhang, Q., Kaltofen, S., Schotta, G., et al. (2014). Specificity, propagation, and memory of pericentric heterochromatin. Mol. Syst. Biol. *10*, 746.

Pan, Q., Shai, O., Lee, L.J., Frey, B.J., and Blencowe, B.J. (2008). Deep surveying of alternative splicing complexity in the human transcriptome by high-throughput sequencing. Nat. Genet. *40*, 1413–1415.

Piacentini, L., Fanti, L., Negri, R., Del Vescovo, V., Fatica, A., Altieri, F., and Pimpinelli, S. (2009). Heterochromatin protein 1 (HP1a) positively regulates

euchromatic gene expression through RNA transcript association and interaction with hnRNPs in Drosophila. PLoS Genet. *5*, e1000670.

Pradeepa, M.M., Sutherland, H.G., Ule, J., Grimes, G.R., and Bickmore, W.A. (2012). Psip1/Ledgf p52 binds methylated histone H3K36 and splicing factors and contributes to the regulation of alternative splicing. PLoS Genet. *8*, e1002717.

Rauch, T.A., Wu, X., Zhong, X., Riggs, A.D., and Pfeifer, G.P. (2009). A human B cell methylome at 100-base pair resolution. Proc. Natl. Acad. Sci. USA *106*, 671–678.

Rhyasen, G.W., Bolanos, L., Fang, J., Jerez, A., Wunderlich, M., Rigolino, C., Mathews, L., Ferrer, M., Southall, N., Guha, R., et al. (2013). Targeting IRAK1 as a therapeutic approach for myelodysplastic syndrome. Cancer Cell *24*, 90–104.

Saint-André, V., Batsché, E., Rachez, C., and Muchardt, C. (2011). Histone H3 lysine 9 trimethylation and HP1γ favor inclusion of alternative exons. Nat. Struct. Mol. Biol. *18*, 337–344.

Schor, I.E., Fiszbein, A., Petrillo, E., and Kornblihtt, A.R. (2013). Intragenic epigenetic changes modulate NCAM alternative splicing in neuronal differentiation. EMBO J. *32*, 2264–2274.

Schwartz, S., Meshorer, E., and Ast, G. (2009). Chromatin organization marks exon-intron structure. Nat. Struct. Mol. Biol. *16*, 990–995.

Shukla, S., Kavak, E., Gregory, M., Imashimizu, M., Shutinoski, B., Kashlev, M., Oberdoerffer, P., Sandberg, R., and Oberdoerffer, S. (2011). CTCF-promoted RNA polymerase II pausing links DNA methylation to splicing. Nature *479*, 74–79.

Sims, R.J., 3rd, Millhouse, S., Chen, C.F., Lewis, B.A., Erdjument-Bromage, H., Tempst, P., Manley, J.L., and Reinberg, D. (2007). Recognition of trimethylated histone H3 lysine 4 facilitates the recruitment of transcription postinitiation factors and pre-mRNA splicing. Mol. Cell *28*, 665–676.

Smallwood, A., Hon, G.C., Jin, F., Henry, R.E., Espinosa, J.M., and Ren, B. (2012). CBX3 regulates efficient RNA processing genome-wide. Genome Res. *22*, 1426–1436.

Smith, Z.D., and Meissner, A. (2013). DNA methylation: roles in mammalian development. Nat. Rev. Genet. *14*, 204–220.

Takanashi, M., Oikawa, K., Fujita, K., Kudo, M., Kinoshita, M., and Kuroda, M. (2009). Heterochromatin protein 1gamma epigenetically regulates cell differentiation and exhibits potential as a therapeutic target for various types of cancers. Am. J. Pathol. *174*, 309–316.

Tilgner, H., Nikolaou, C., Althammer, S., Sammeth, M., Beato, M., Valcárcel, J., and Guigó, R. (2009). Nucleosome positioning as a determinant of exon recognition. Nat. Struct. Mol. Biol. *16*, 996–1001.

Tiwari, V.K., Burger, L., Nikoletopoulou, V., Deogracias, R., Thakurela, S., Wirbelauer, C., Kaut, J., Terranova, R., Hoerner, L., Mielke, C., et al. (2012). Target genes of Topoisomerase IIβ regulate neuronal survival and are defined by their chromatin state. Proc. Natl. Acad. Sci. USA *109*, E934–E943.

Tsumura, A., Hayakawa, T., Kumaki, Y., Takebayashi, S., Sakaue, M., Matsuoka, C., Shimotohno, K., Ishikawa, F., Li, E., Ueda, H.R., et al. (2006). Maintenance of self-renewal ability of mouse embryonic stem cells in the absence of DNA methyltransferases Dnmt1, Dnmt3a and Dnmt3b. Genes Cells *11*, 805–814.

Wang, E.T., Sandberg, R., Luo, S., Khrebtukova, I., Zhang, L., Mayr, C., Kingsmore, S.F., Schroth, G.P., and Burge, C.B. (2008). Alternative isoform regulation in human tissue transcriptomes. Nature *456*, 470–476.

Cell Reports

Supplemental Information

HP1 Is Involved in Regulating the Global Impact of DNA Methylation on Alternative Splicing

Ahuvi Yearim, Sahar Gelfman, Ronna Shayevitch, Shai Melcer, Ohad Glaich, Jan-Philipp Mallm, Malka Nissim-Rafinia, Ayelet-Hashahar S. Cohen, Karsten Rippe, Eran Meshorer, and Gil Ast

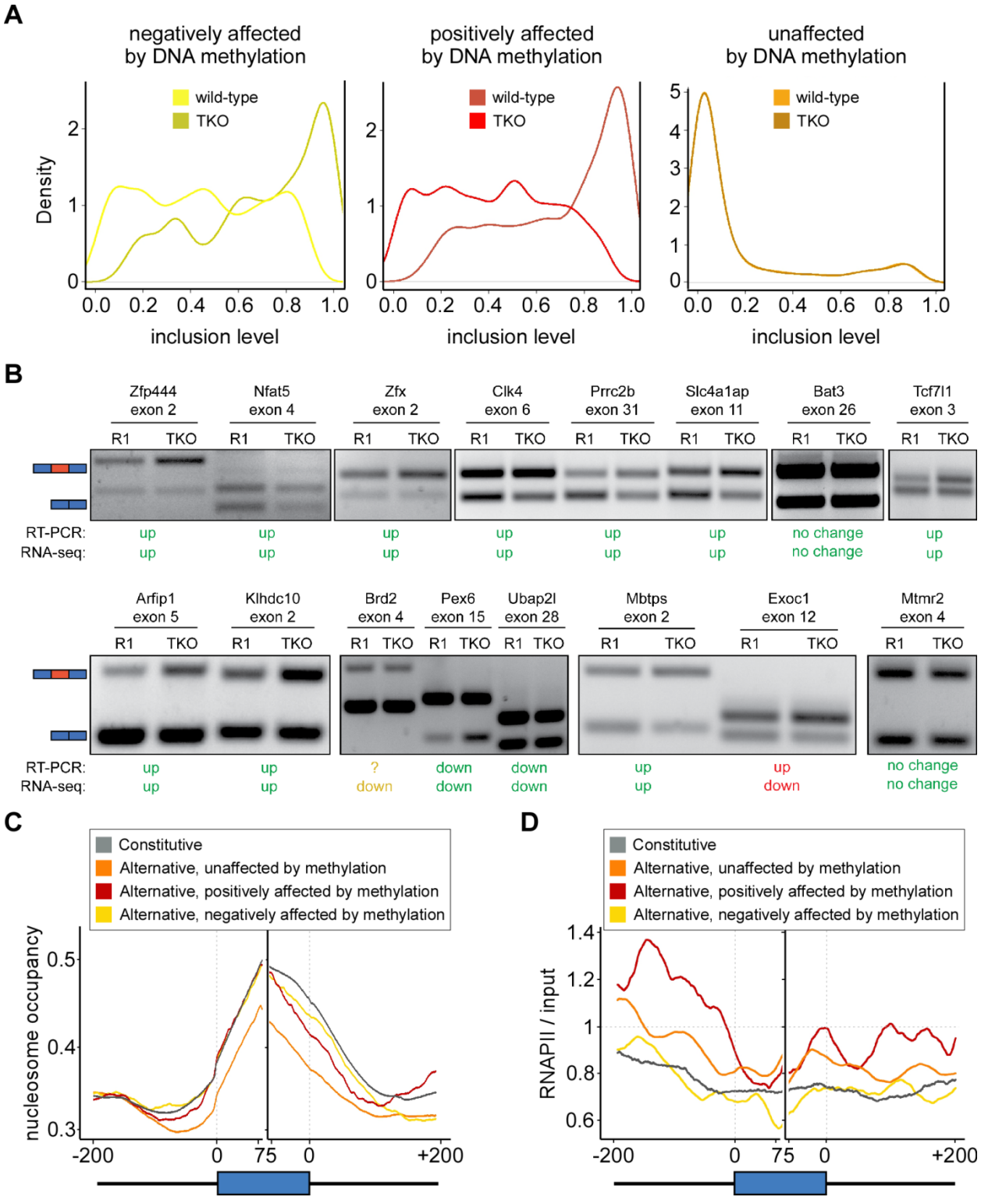

Figure S1. Altered DNA methylation patterns affect alternative splicing globally – additional data, related to Figure 1. (**A**) Density distribution of inclusion level of exons

affected by DNA methylation. Density distributions of alternative exons are shown for both wild-type and TKO cells. (**B**) Validation of RNA-seq results. RT-PCR analysis of RNA from wild-type (R1) and TKO cells for 16 alternative cassette exons. For each alternative event inclusion and skipping of the cassette exon result in upper and lower bands, respectively. Below the gels are indicators whether inclusion levels were higher (up) or lower (down) in TKO cells relative to R1 cells in both RT-PCR and RNA-seq analyses. Indicators are colored green if RT-PCR and RNA-seq were similar and red if they differed. (**C**) Nucleosome occupancy levels of exon groups in TKO cells. The average value was calculated per base for exons (75 nucleotides from each splice site) and flanking intronic regions (200 nucleotides) and a running average of 20- nucleotide windows was applied. (**D**) Normalized ChIP-seq values of RNA Polymerase II based on the effect of DNA methylation on splicing. RNA Polymerase II (RNAPII) ChIP was divided by input in wild-type cells, and measured along the upstream intron, exon, and downstream intron regions.

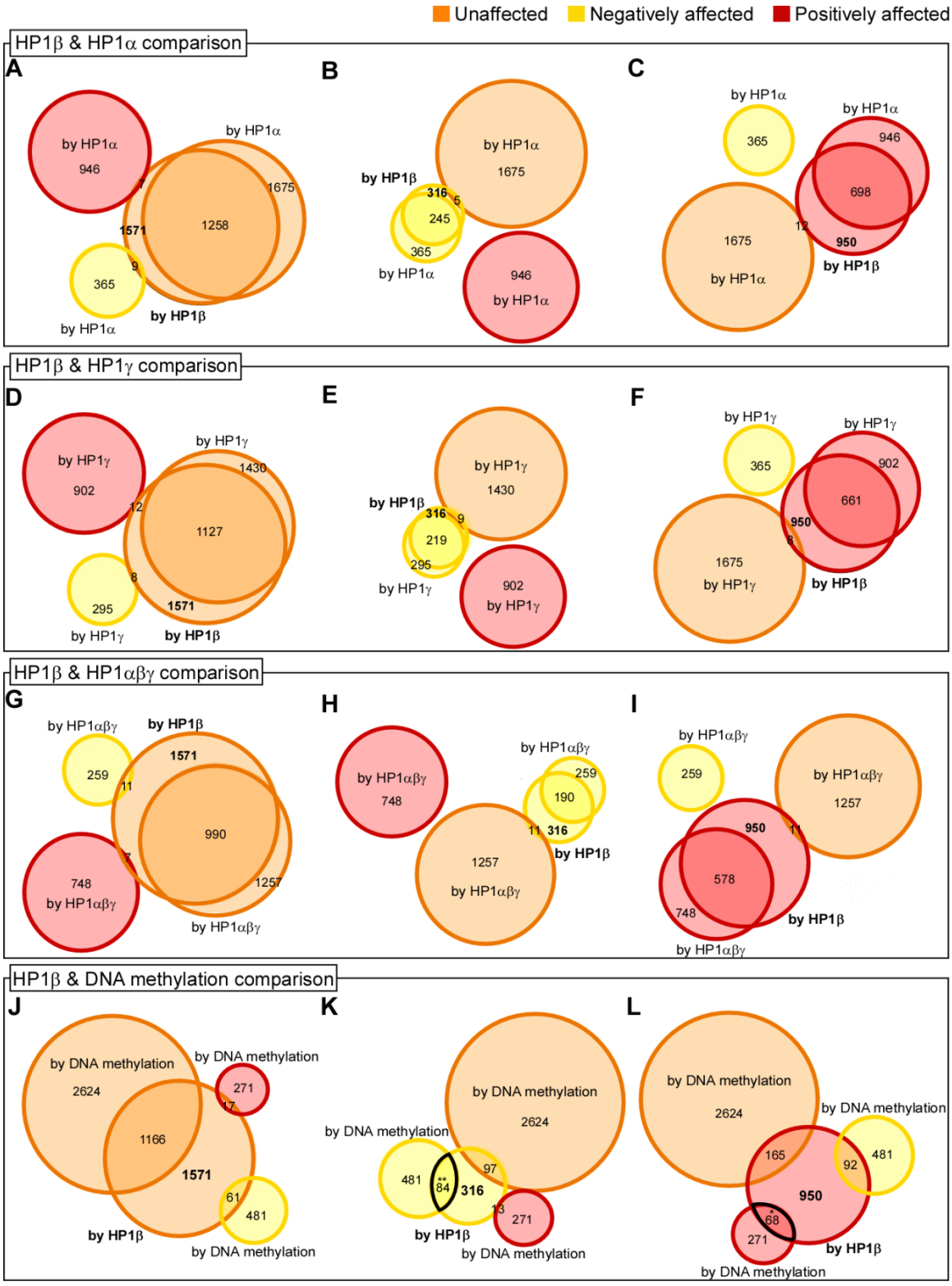

Figure S2. Overlaps of exon populations affected by different HP1 isoforms and DNA methylation, related to Figure 2. (**A**) Overlap between alterative exons that retained the same

inclusion in cells treated with HP1β siRNA (orange, in bold) with alterative exons that retained (orange), increased (yellow), and decreased (red) inclusion in cells treated with HP1α siRNA. (**B**) Overlap between alterative exons that increased inclusion in cells treated with HP1β siRNA (yellow, in bold) with alterative exons that retained (orange), increased (yellow), and decreased (red) inclusion in cells treated with HP1α siRNA. (**C**) Overlap between alterative exons that decreased inclusion in cells treated with HP1β siRNA (red, in bold) with alterative exons that retained (orange), increased (yellow), and decreased (red) inclusion in cells treated with HP1α siRNA. (**D**)-(**F**) Same as panels (A-C) but for comparison between HP1β siRNA (in bold) with HP1γ siRNA. (**G**)-(**I**) Same as panels (A-C) but for comparison between HP1β siRNA (in bold) with cells treated with siRNA targeting each of the three HP1 isoforms (HP1αβγ). (**J**)-(**L**) Same as panels (A-C) but for comparison between HP1β siRNA (in bold) with methylation-deficient TKO cells. *proportions test, $P < 1.3\times10^{-14}$; **proportions test, $P < 2.2\times10^{-16}$.

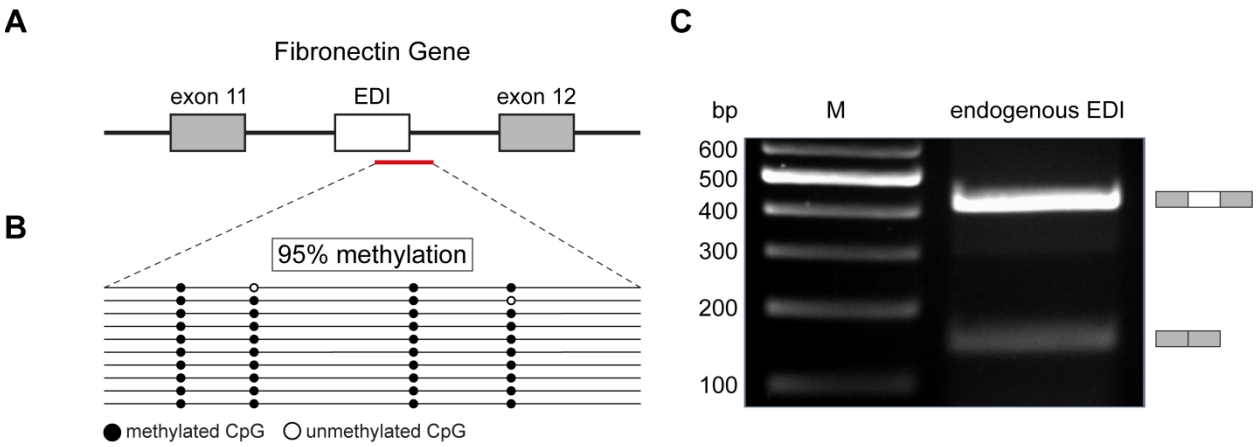

Figure S3. Characterization of endogenous EDI methylation and splicing patterns, related to Figure 3. (**A**) Schematic diagram of the endogenous Fibronectin gene region containing the EDI segment. Grey and white boxes indicate exons and lines indicate introns. (**B**) Bisulfate sequencing of the representative region (in red) on genomic DNA from Flp-In-HEK293 cells (without the EDI minigene). Total methylation percentage of the region is presented above the plot. (**C**) RT-PCR of RNA from Flp-In-HEK293 cells (without the EDI minigene). The upper and lower bands represent inclusion and skipping of the endogenous alternative EDI segment.

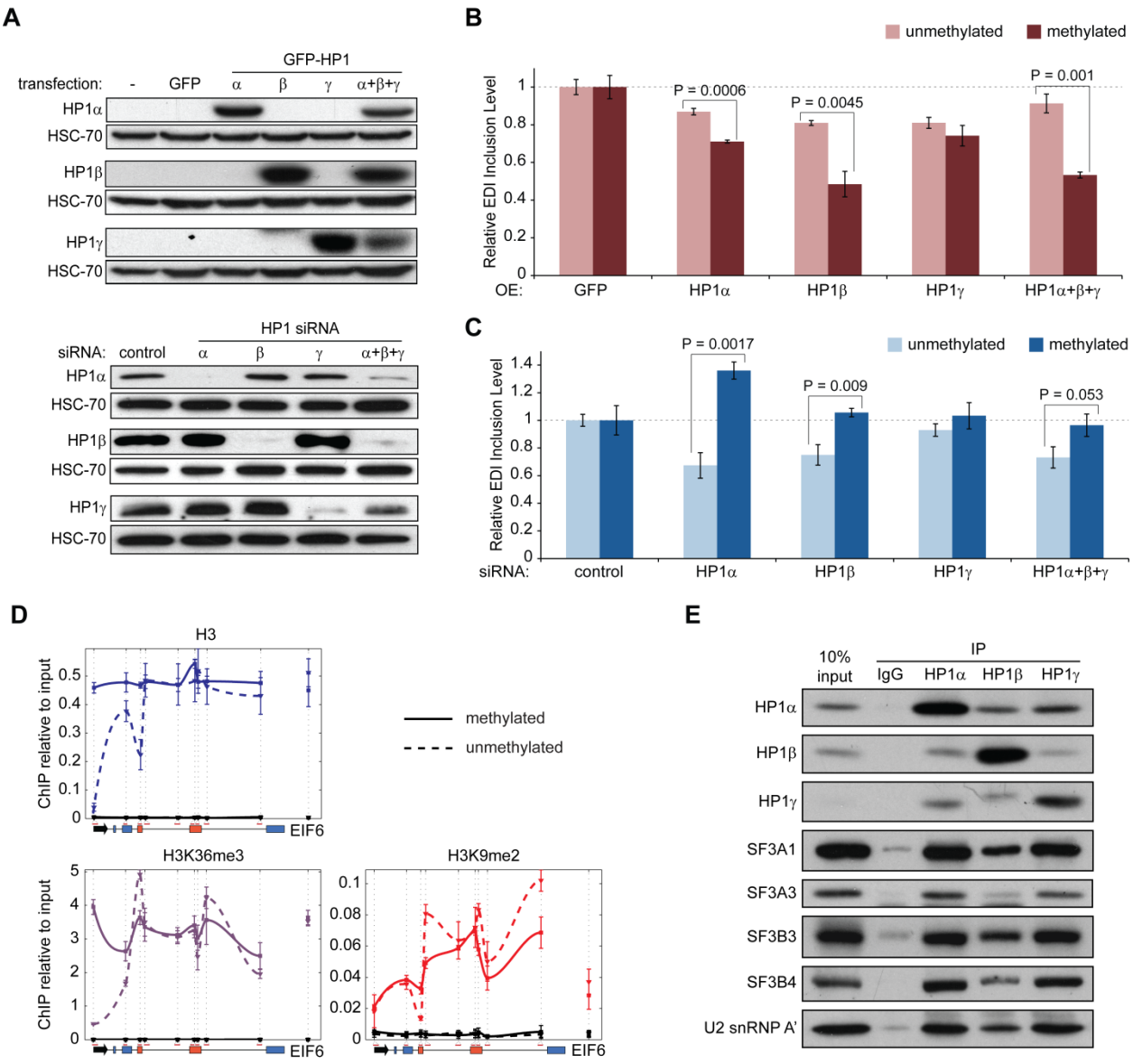

Figure S4. The HP1 mechanism – additional data, related to Figure 4. (**A**) Western blot analysis of HP1 after over-expression or siRNA knock-down. HSC-70 was used as loading control. (**B**) qRT-PCR analysis using the previously indicated exon-exon junction primers to assess EDI inclusion levels in cells that over-express HP1 or GFP (n = 3). (**C**) qRT-PCR analysis to assess EDI inclusion levels in cells treated with HP1 siRNA or control siRNA (n = 3). (**D**) ChIP of H3, H3K9me2, and H3K36me3 in cells containing unmethylated and methylated EDI and quantitative PCR along the EDI minigene. The EIF6 intron 3 region was used for

endogenous background control. Values represent the mean ± SEM of ChIP relative to input (n = 3). Dotted and full lines represent ChIP signal in cells containing unmethylated and methylated EDI, respectively. Black lines represent ChIP with rabbit IgG. All graphs show mean values ± SEM. Student's *t* test was used to compare the indicated samples. (**E**) HP1 is associated to U2 snRNP components: Co-IP of HP1 isoforms with various U2 snRNP components in Flp-In-HEK293 cells.

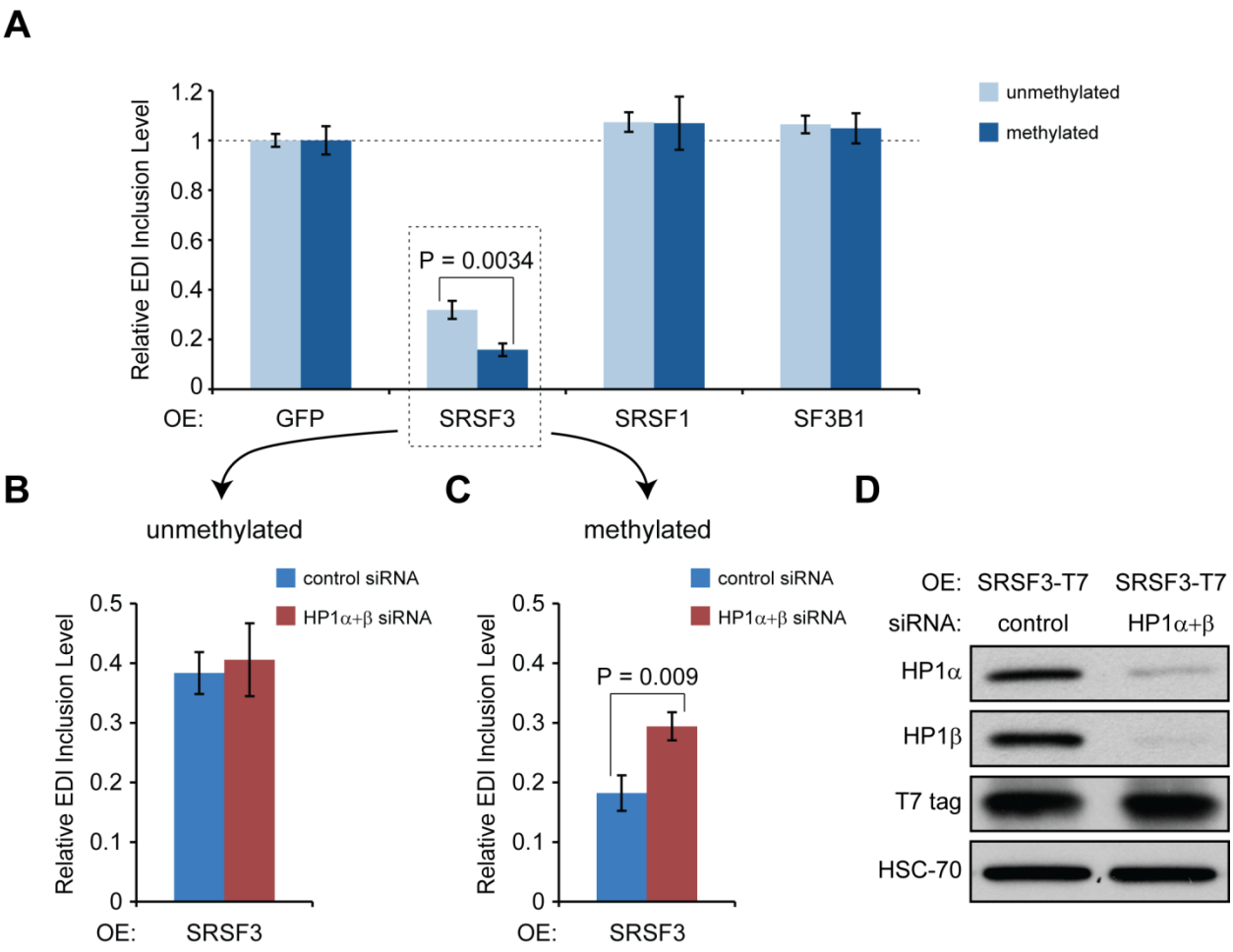

Figure S5. SRSF3 over-expression silences methylated EDI's inclusion in an HP1-dependent fashion, related to Figure 4. (**A**) qRT-PCR analysis to assess EDI inclusion levels in cells that over-express (OE) indicated splicing factors or GFP (n = 5). (**B**) SRSF3 (or GFP) was over-expressed and cells were treated with HP1 siRNA (red) or control siRNA (blue). EDI inclusion levels were determined for SRSF3 over-expression relative to GFP over-expression in unmethylated cells (n = 5). (**C**) Same as panel (B) but for methylated cells (n = 5). (**D**) Western blot analysis of exogenous levels of SRSF3 (measured by T7 tag antibody) in cells treated with HP1 or control siRNA. HSC-70 was used as loading control. All graphs show mean values ± SEM. Student's *t* test was used to compare the indicated samples.

Table S1. Gene expression levels of spliceosomal proteins based on previously published data (Hegele et al., 2012; Wahl et al., 2009). See attached Excel file. Related to Figure 1

Table S2. Gene expression levels of all mouse proteins. See attached Excel file. Related to Figure 1

Supplemental Experimental Procedures

Cells

Flp-In-HEK293 cells were obtained from Invitrogen and were cultured in complete DMEM medium (DMEM high glucose (Sigma), 10% fetal bovine serum (Sigma), 2 mg/ml L-alanyl-L-glutamine (Biological Industries Israel), 100 U/ml penicillin, 0.1 mg/ml streptomycin (Biological Industries Israel)), supplemented with 50 µg/ml Zeocin (Invitrogen). Flp-In-HEK293-EDI stable cells were cultured in complete DMEM medium supplemented with 100 µg/ml hygromycin B (InvivoGen). Mouse R1 ESCs were from ATCC. Dnmt triple knockout (TKO) ESCs were a kind gift from Prof. Masaki Okano (RIKEN) and have been previously described (Tsumura et al., 2006). Mouse ESCs were cultured in ESC medium (DMEM high glucose (Sigma), 15% ES cell qualified heat inactivated FBS (Biological Industries Israel), 0.1 mM non-essential amino acids (Biological Industries Israel), 1 mM sodium pyruvate (Biological Industries Israel), 100 µM β-mercaptoethanol (Sigma), 100 U/ml penicillin, 0.1 mg/ml streptomycin (Biological Industries Israel), 2.28 mM L-alanyl-L-glutamine (Biological Industries Israel), and 1,000 U/ml LIF (Sigma)). Mouse ESCs were grown without MEFs on gelatin-coated plates, and media was changed daily. All cells were grown at 37 °C in a humidified atmosphere with 5% CO_2.

Subcloning of plasmids for creation of stable cell lines

pSVEDA/FN (EDI minigene) was a kind gift from Prof. Alberto Kornblihtt (Universidad de Buenos Aires) and has been previously described (Cramer et al., 1999). pcDNA5/FRT/TO (pFRT, Invitrogen) was used in order to introduce a gene of interest into Flp-In cell lines using Flp recombinase mediated homologous recombination. In order to switch the CMV promoter in pFRT to a fibronectin (FN) promoter we performed a PCR reaction on pFRT to amplify the

plasmid sequence without the CMV promoter region using Phusion High-Fidelity DNA Polymerase (NEB) and primers with 5' tails carrying restriction digestion sites for BstBI and AgeI (forward, 5'-AAAAAA-TTCGAA-GCAGAGCTCTCCCTATCAGTG-3'; reverse, 5'-AAAAAA-ACCGGT-GCGTATATCTGGCCCGTACAT-3'). A PCR reaction was performed on pSVEDA/FN to amplify its FN promoter sequence using primers with 5' tails carrying restriction digestion sites for AgeI and BstBI (forward, 5'-AAAAAA-ACCGGT-ATTCGAGCTCGGTACCCTATG-3'; reverse, 5'-AAAAAA-TTCGAA-AGCTTGGGGTTCCCTCTCC-3'). PCR products were purified using Wizard Plus SV Miniprep DNA Purification System (Promega), digested with AgeI and BstBI, and ligated together using Rapid DNA Dephos & Ligation Kit (Roche). The product plasmid pFRT-FN contained all the features of pFRT with an FN promoter. The EDI minigene was introduced into pFRT-FN by simple AflII and BamHI subcloning to create the pFRT-FN-EDI plasmid.

Generating EDI stable cell lines

pFRT-FN-EDI was methylated *in vitro* using M.SssI (NEB). The methylation reaction was verified by digestion of a sample with the methylation-sensitive restriction enzyme BstUI (NEB) followed by agarose gel electrophoresis. Plasmids were purified using Wizard Plus SV Minipreps DNA Purification System (Promega). For transfection, 2-3×10^5 Flp-In-HEK293 cells (Invitrogen) were seeded in 30-mm plates in complete DMEM medium (without zeocin). The following day cells were co-transfected with 4.5 µg pOG44 (Flp recombinase expression vector, Invitrogen) and 0.5 µg pFRT-FN-EDI (*in vitro* methylated or unmethylated) in a 9:1 Flp recombinase to EDI minigene ratio using TransIT-LT1 reagent (Mirus). After 48 hours cells were transferred to 15-cm plates and were grown to 10-20% confluence. Cells were maintained for 2-3 weeks in complete DMEM supplemented with 100 µg/ml hygromycin B (InvivoGen).

Medium was replaced every 3-4 days until resistant foci were observed. Several foci (colonies) were transferred to 30-mm plates, each colony representing a monoclonal stable cell line. These monoclonal stable cell lines were further expanded for 1-2 weeks in complete DMEM supplemented with 100 µg/ml hygromycin B.

EDI Bisulfite sequencing

DNA was extracted from cells using High Pure PCR Template Preparation kit (Roche). Approximately 600 ng of DNA was bisulfite (BS) converted using EZ DNA Methylation kit (Zymo). This DNA was used as a template for PCR using FastStart High Fidelity PCR system (Roche) and specially designed primers, listed in a table below. This reaction was run on a thermocycling program for 35 cycles where each cycle was consisted of 30 seconds at 95 ºC, 30 seconds at 58 ºC, and 35 seconds at 72 ºC. The PCR product was cloned into a plasmid using TOPO TA cloning kit (Invitrogen) and transformed into XL10-Gold cells. DNA was extracted using Wizard Plus SV Minipreps DNA Purification System (Promega) and sequenced using the forward primer from the PCR reaction. Data analysis and lollipop diagrams were generated using BiQ Analyzer software (Bock et al., 2005).

Analysis of splicing patterns by RT-PCR and quantitative RT-PCR (qRT-PCR)

Total RNA was extracted from the cells with TRI reagent (Sigma) according to the manufacturers' instructions. Approximately 2 µg of total RNA was reverse transcribed with SuperScript III First-Strand Synthesis System for RT-PCR (Invitrogen) using an oligo$(dT)_{20}$ primer. For RT-PCR of EDI alternative splice product and for validation of RNA-seq, PCR was performed using Biotools DNA Polymerase (Biotools) on a Biometra using the following thermocycling parameters: 2 minutes at 94 ºC followed by 30 cycles of 30 seconds at 94 ºC, 45

seconds at 58 ºC, and 60 seconds at 72 ºC, ending with a final extension of 10 minutes at 72 ºC. For qRT-PCR, qPCR was performed using KAPA SYBR FAST Universal qPCR kit (KAPA Biosystems) using two exon-exon junction primer pairs designed to detect the inclusion isoform and the skipping isoform. To calculate EDI inclusion levels of methylated relative to unmethylated cells from qPCR we used the following equation: $\frac{2^{inclusion\ C_t(unmethylated) - inclusion\ C_t(methylated)}}{2^{skipping\ C_t(unmethylated) - skipping\ C_t(methylated)}}$. qPCR reactions were performed on a Stratagene Mx3005P thermocycler using the following thermocycling parameters: 3 minutes at 95 ºC followed by 40 cycles of 3 seconds at 95 ºC and 30 seconds at 60 ºC, ending with a dissociation curve. Primer sequences are listed in a table below.

Over-expression and siRNA knock-down

Proteins were over-expressed using the TransIT-LT1 system (Mirus). Following transfection, cells were incubated for 48 hours, and then RNA and proteins were extracted. The expression plasmids encoding HP1α-GFP, HP1β-GFP, HP1γ-GFP, SRSF1-T7, and SRSF3-T7 were previously described (Caceres et al., 1997; Cheutin et al., 2003). The expression plasmid encoding the SF3B1-GFP fusion protein was a kind gift from Prof. Juan Valcarcel (Centre de Regulació Genòmica). In all experiments, an empty pEGFP-C3 plasmid was used for control.

Knock-downs were performed using siGENOME siRNAs (Dharmacon). Flp-In-HEK293-EDI cells were transfected with siRNAs using Lipofectamine RNAiMAX (Invitrogen). Following transfection, cells were incubated for 96 hours, and then RNA and proteins were extracted. The siRNA concentration was 60 nM. In R1 and TKO cells transfections were performed using Lipofectamine 2000 (Invitrogen). Following transfection, cells were incubated for 48 hours before RNA and proteins were extracted. The siRNA concentration used in R1 cells was 90 nM

for individual siRNAs and 60nM each siRNA when all three isoforms were targeted in a single experiment. In TKO cells, 80 nM HP1α siRNA, 80 nM HP1β siRNA, and 120 nM HP1γ siRNA were used for knock-down of all three isoforms. Guide strand siRNA sequences were: Control siRNA, siGENOME non-targeting human siRNA pool #2; human HP1α siRNA, 5'-CCUGAGAAAAACUUGGAUUdTdT-3'; mouse HP1α siRNA, 5'-CACAGAUUGUGAUAGCAUUdTdT-3'; human/mouse HP1β siRNA, 5'-AGCUCAUGUUCCUGAUGAAdTdT-3'; human/mouse HP1γ siRNA, 5'-AUCUGACAGUGAAUCUGAUdTdT-3'; human SRSF3 siRNA, 5'-CGAUCUAGGUCAAAUGAAA-3'.

Co-immunoprecipitation and western blotting

Flp-In-HEK293 cells (4-5×10^7 cells per sample) were pelleted by centrifugation and washed with PBS. Nuclei were purified by re-suspending the pellet in Nuc Buffer (15 mM Tris-HCl, pH 7.5, 60 mM KCl, 15 mM NaCl, 5 mM $MgCl_2$, 0.1 mM EGTA, 0.2% (v/v) NP-40 (Sigma IGEPAL), 1 mM DTT, 0.1 mM PMSF (Sigma), complete protease inhibitor cocktail (Roche)) and incubating on ice for 7 minutes. Cells were layered on a sucrose cushion and centrifuged for 20 minutes at 12,000 g to separate the nuclei from the NP-40 detergent. The supernatant was removed, and the purified nuclei were re-suspended in MNase Digestion Buffer (0.32 M sucrose, 50 mM Tris-HCl, pH 7.5, 4 mM $MgCl_2$, 1 mM $CaCl_2$, 0.1 mM PMSF (Sigma)) with 50 units of MNase (Worthington) and incubated at 37 ºC for 5 minutes in order to release chromatin-bound proteins. The reaction was stopped by addition of 50 mM EDTA and was centrifuged for 10 minutes at 10,000 g. The pellet was re-suspended in IP Buffer (20 mM Tris-HCl, pH 8.1, 150 mM NaCl, 1 mM EDTA, 1 mM EGTA, 1% Triton X-100, 0.1% deoxycholic acid, 0.1% SDS, complete protease inhibitor cocktail (Roche), 0.1 mM PMSF (Sigma)) and aliquoted into

immunoprecipitation (IP) and input fractions. Appropriate antibody (4 µg normal rabbit IgG, HP1α, HP1β, HP1γ) was added and IPs were incubated for 16 hours on a rotator at 4 ºC. An aliquot of 50 µl pre-washed protein-A dynabeads (Invitrogen) was added to each sample, and samples were incubated for another 4 hours. Samples were washed four times with IP Buffer and once with RNase A Buffer (PBS (Sigma), 0.02% Tween 20 (Sigma), complete protease inhibitor cocktail (Roche), 0.1 mM PMSF (Sigma)). Samples were resuspended in RNase A Buffer with 1 µl of 10 mg/ml RNase A (Sigma) and incubated for 30 minutes at 37 ºC. Samples were washed three times with IP Buffer. Protein was eluted from the beads by adding SDS sample buffer and incubating in a thermo-shaker for 15 minutes at 75 ºC with vigorous shaking. The supernatant was boiled for another 5 minutes at 100 ºC. Proteins were separated by SDS-PAGE on 4-20% polyacrylamide gradient gels and transferred to nitrocellulose membranes (Whatman Protran 0.45 µm). The membranes were incubated with the appropriate primary and secondary antibodies and washed with TBS-Tween 20. Horseradish peroxidase conjugated secondary antibodies were detected by SuperSignal West Pico Chemiluminescent Substrate (Thermo Scientific). The antibodies and concentrations used are listed in a table below.

Chromatin immunoprecipitation (ChIP)

Approximately 4×10^7 cells per sample were cross-linked for 10 minutes in 1% formaldehyde. Cross-linking was quenched by the addition of 125 mM glycine. Cells were washed twice with PBS, centrifuged, and pellets were frozen at -80 ºC. Pellets were thawed on ice, resuspended in Lysis Buffer (1% SDS, 10 mM EDTA, 50 mM Tris-HCl, pH 8.1, complete protease inhibitor cocktail (Roche)) and sonicated with a Vibra-Cell VCX600 (Sonics & Materials) to obtain an average DNA length of 150-350 bp. After centrifugation at 20,000 g for 8 minutes, the supernatant was diluted 1:10 with Dilution Buffer (0.01% SDS, 1.1% Triton X-100, 1.2 mM

EDTA, 16.7 mM Tris-HCl, pH 8.1, 167 mM NaCl, complete protease inhibitor cocktail (Roche)) and aliquoted for IP; chromatin from an equivalent of 4×10^6 cells was used per IP reaction. Input material was also aliquoted for later analysis. For each IP, 40 µl of protein-A dynabeads (Invitrogen), previously incubated with 4 µg of the antibody of interest, were added, and samples were incubated for 16 hours at 4 ºC. The antibodies used are listed in a table below. The beads were washed six times with RIPA buffer (0.1% deoxycholate, 0.1% SDS, 1% Triton X-100, 10 mM Tris-HCl, pH 8.1, 1 mM EDTA, 140 mM NaCl), twice with RIPA-high salt buffer (0.1% deoxycholate, 0.1% SDS, 1% Triton X-100, 10 mM Tris-HCl, pH 8.1, 1 mM EDTA, 360 mM NaCl), twice with LiCl wash buffer (250 mM LiCl, 0.5% NP-40 (Sigma IGEPAL), 0.5% deoxycholate, 1 mM EDTA, 10 mM Tris-HCl, pH 8.1) and twice with TE buffer (10 mM Tris-HCl, pH 8.1, 1 mM EDTA). DNA was eluted from the beads with Elution buffer (0.5% SDS, 300 mM NaCl, 5 mM EDTA, 10 mM Tris-HCl, pH 8.1) using a 30-minute incubation in a thermo-shaker at 65 ºC. From this stage on, input tubes were processed similarly to elution tubes: 1 µl of 10 mg/ml RNase A (Sigma) was added to the supernatant, and samples were incubated for 30 minutes at 37 ºC; 1.5 µl Proteinase K (NEB) was added and samples were incubated for 16 h at 65ºC. DNA was purified using MinElute PCR purification kit (Qiagen). qPCR was performed using Absolute Blue QPCR SYBR Green ROX Mix (Thermo Scientific). qPCR reactions were run on a Stratagene Mx3005P thermocycler using the following thermocycling parameters: 15 minutes at 95 ºC followed by 40 cycles of 30 seconds at 95 ºC, 45 seconds at 60 ºC and 45 seconds at 72 ºC, ending with a dissociation curve. The qPCR primers used are listed in a table below.

RNA-seq library preparation for splicing analysis

Total RNA was extracted from the cells using TRI reagent (Sigma). Deep sequencing libraries were prepared using standard Illumina TruSeq library preparation kits. Sequencing of 50-bp single-end reads was performed using an Illumina Genome Analyzer II and 2 x 101-bp paired-end sequencing was performed using an Illumina HiSeq 2000.

BS-seq library preparation for DNA methylation mapping

Genomic DNA (5 µg) was extracted from R1 and TKO cells using High Pure PCR Template Preparation kit (Roche). The DNA was fragmented using Covaris S2 (duty cycle: 20%, intensity: 5, cycles/burst: 200, time: 60 seconds) in 130 µl low-EDTA TE buffer to 250-300 bp fragment size. Samples were concentrated by centrifugation on a Speedvac at room temperature. End repair, adenylation, and ligation were performed according to the Illumina protocol using Illumina methylated adaptors. Adapter-ligated DNA of 200-240 bp was isolated using 2% E-gels and samples were concentrated on a Speedvac at room temperature. Bisulfite conversion was performed with EZ DNA methylation kit (Zymo Research), and DNA was eluted with 30 µl elution buffer. The eluate was aliquoted for six parallel PCR reactions, yielding six independent libraries from the same biological samples. This reduced the incidence of “clonal” reads, reads that share the same alignment position and likely originate from the same template molecule. PCR was performed using Fast Start High Fidelity PCR system (Roche) using the following thermocycling parameters: 2 minutes at 95 ºC followed by 8 cycles of 30 seconds at 95 ºC, 20 seconds at 65 ºC and 45 seconds at 72 ºC, ending with a final extension of 7 minutes at 72 ºC. The PCR products were pooled and purified using Agencourt AMPure XP (Beckman Coulter), and 2 x 100-bp paired-end sequencing was performed using an Illumina HiSeq 2000.

MNase-seq library preparation for nucleosome mapping

Approximately 4×10^7 R1 or TKO cells were cross-linked for 10 minutes in 0.5% formaldehyde. Cross-linking was quenched by addition of 125 mM glycine. Nuclei were purified using a protocol similar to that used for co-immunoprecipitation experiments, but using 0.025% (v/v) NP-40 instead of 0.2%. The purified nuclei were re-suspended in 0.5 ml MNase Digestion Buffer (see co-immunoprecipitation section) with 160 units of MNase (Worthington) and incubated at 37 ºC for 10 minutes to achieve a digestion efficiency of ~90% mononucleosomes. The reaction was stopped by addition of 60 µl 50 mM EDTA, 25 µl 5 M NaCl, and 15 µl 20% NP-40 and incubated on a rotator for 1 hour at room temperature to release soluble nucleosomes. The reaction was centrifuged for 5 minutes at 10,000 g, and the supernatant, containing soluble nucleosomes without nuclear debris, was moved to a new tube. Proteinase K (1.4 µl, NEB) and SDS (0.5% final concentration) were added and the reaction was incubated for 16 hours at 65 ºC. DNA was purified using Wizard SV gel and PCR cleanup system (Promega) and eluted with 50 µl PBS (Sigma). RNase A (1 µl of a 10 mg/ml stock, Sigma) was added and the reaction was incubated for 2 hours at 37 ºC. The reaction was loaded on a 1.5% agarose gel and the ~150-bp mononucleosome band was excised from the gel and purified using Wizard SV gel and PCR cleanup system (Promega). Deep sequencing libraries were prepared using standard Illumina ChIP-seq library prep kits and 36-40-bp single-end sequencing was performed using an Illumina Genome Analyzer II.

RNA-seq computational analyses

RNA-seq experiments were performed on RNA isolated from wild-type R1 and TKO mouse ES cells and from R1 cells and TKO cells treated with siRNAs targeting HP1 isoforms. Two

biological replicates of non-treated cells and two technical replicates for each biological replicate of siRNA-treated cells were obtained. Technical replicates were compared using CuffDiff (Trapnell et al., 2010) and were found 99.9% identical. We then united the technical replicates. Biological replicates had similarities of 99.7%; biological replicates were thus united for a stronger statistical power when identifying alternative exons. We then mapped the pooled Fastq files to the mouse genome (mm10) using Tophat2 (Kim et al., 2013) and Bowtie2 (Langmead and Salzberg, 2012). For RNA-seq mapping statistics see table below.

The MISO tool (Katz et al., 2010) was used to estimate inclusion levels of 14,959 exons using the 'run_events_analysis.py --compute-genes-psi' function, based on the SE.mm10.gff3 MISO dataset of verified alternative exons (Katz et al., 2010). We used a prefilter threshold value of 100 read coverage for MISO calculation of the number of reads in the input BAM that map to each event. Events that did not meet the read coverage thresholds were removed.

We compared different RNA-seq experiments using the MISO 'compare-samples' function, thus obtaining inclusion level differences, statistical significance, and Bayes factor of the results. Exons with altered inclusion levels were selected based on the following conditions: 1) inclusion level lower than 90% in both conditions, 2) at least 10% difference between two conditions in the required direction (positive difference = increase, negative difference = decrease), and 3) Bayes factor > 2. Unchanged exons were selected based on the following conditions: 1) inclusion level lower than 90% in both conditions, 2) maximum absolute difference of 5% between conditions, and 3) Bayes factor ≤ 1.

Differential expression between wild-type and TKO cells

We used the full list of 244 human spliceosomal and regulatory protein coding genes as depicted by Wahl et al (Wahl et al., 2009) and obtained from Hegele et al. (Hegele et al., 2012). 217 mouse genes that are homologous to the 244 human genes were extracted based on the human-mouse homology table from the Mouse Genome Informatics site of the Jackson Laboratory (www.informatics.jax.org/homology.shtml). The differential expression of these genes between wild-type and TKO cells was examined using the CuffDiff tool (Trapnell et al., 2010). A significant change in expression between the two samples was decided based on the FDR corrected (5%) *p-value* of the statistical test between the samples that is issued by the CuffDiff tool.

Conservation score calculation

We calculated average conservation values using the 60-way Phastcons values (Siepel et al., 2005) that were obtained from the UCSC genome browser (http://hgdownload-test.sdsc.edu/goldenPath/mm10/phastCons60way/mm10.60way.phastCons/).

BS-seq computational analyses

BS-seq experiments were performed for mouse R1 cells. Fastq files were mapped to the mouse genome (mm10) using the Bismark tool (Krueger and Andrews, 2011) and Bowtie (Langmead et al., 2009) with default settings (for BS-seq mapping statistics see table below). CpG methylation was extracted from the mapped data using the 'Bismark methylation extractor' function and converted to Bedgraph files using Bismark's 'myBedConverter' function.

Next, the level of methylated CpGs was calculated per exon and flanking regions for increased, decreased, and unchanged alternative exons as well as for a group of 68,835 verified constitutive exons that were neither first nor last in a gene. mCpG/CpG patterns on exons and flanking regions were calculated as previously described (Gelfman et al., 2013): Single-base resolution values were cast upon sets of exons and introns using the 'cast data' function constructed in our lab. 'Cast data' constructs two datasets for the two splice sites: One is centered on the 3' splice site and the other on the 5' splice site. All sequences were aligned to the plus strand, thus methylation values of an exon that is coded on the minus strand were reversed. The exon-intron strip contained 75 nt of exon sequence from each splice site and 200 nt of intronic sequence from each side of each exon. Exons that were shorter than 75 nt received a null value for the remaining positions, and the same was done for introns shorter than 200 nt. It is important to note that this method results in duplication of data for exons that are shorter than 150 nt. For example, for an exon with the length of 100 nt, positions 1 to 75 will be used for display at the 3' splice site end of the exon, whereas positions 25 to 100 will be used for display at the 5' splice site end of the exon. We used this method in order to be faithful to the true values with regard to each splice site and not to the middle of the exon. Scripts were written using the perl script language and the R statistical computing program (Team, 2006).

Calculation of the mCpG/CpG ratio was also done as previously described (Gelfman et al., 2013): the mCpG/CpG value takes into account the read count of DNA-methylation and the CpG abundance at a certain position relative to the exon-intron junction of all measured exons. All exons were positioned relative to the splice sites, allowing the extraction of only exons/introns that have a CG dinucleotide in the examined position. Average methylation levels were calculated only for these cases.

MNase-seq computational analyses

MNase-seq experiments were performed for mouse R1 and TKO cells. Fastq files of three biological replicates per each condition were mapped to the mouse genome (mm10) using Bowtie2 (Langmead and Salzberg, 2012) with default settings (for MNase-seq mapping statistics see table below). We constructed a perl script that calculates a single score for 73 bp from the start of the read, thus creating .wg files containing the marking of a single position as the center of the fragment/nucleosome. Data was then cast upon exon-intron structures using our 'cast data' function. Next, in the dataset constructed using 'cast data', each center nucleosome score was expanded 73 bp upstream and downstream, creating a 147-bp segment representing a nucleosome binding site. Scores for each position were averaged for the relevant group of exons (e.g., increased, decreased, unchanged inclusion exons) and flanking regions. Next, we applied a running average of a 10-nt window on the vector of average values for the exon-intron structure.

HP1β ChIP-seq computational analysis

Fastq files were mapped to the mouse genome (mm10) using Bowtie2 (Langmead and Salzberg, 2012) with default settings (for ChIP-seq mapping statistics see table below). We used the same perl script as used for MNase-seq analyses to produce .wg files with read scores for each genomic coordinate. Data was then cast upon exon-intron structures using our 'cast data' function. Scores for each position were averaged in the relevant group of exons (e.g., all exons, short introns, long introns), and average read counts of HP1β samples were normalized to that of the input sample. Next, we applied a running average of 150-nt windows on the vector of average values for the exon-intron structure. We generated normalized HP1β fold enrichment

signals over the exon and introns of each examined group by dividing the calculated reads at each position with the calculated reads based on the input sample.

Statistical analysis for overlap of exons affected by DNA methylation and HP1β

The proportion of affected overlapping exons was calculated as follows: In the case of HP1β affected groups overlapping with DNA methylation positively affected exons: the expected proportion of overlap between TKO positively affected exons and all HP1β groups is 0.096 (325/3,421). However, the observed overlap between just the TKO positively affected group and HP1β positively affected group is 0.25 (68/271), presenting a strong significant multiple of the expected ratio. This multiple was used for a proportions hypothesis test, producing a *p-value* of less than 2.2×10^{-16}. In the other case of HP1β affected groups overlapping with DNA methylation negatively affected exons: the expected proportion of overlap between TKO negatively affected exons and all HP1β groups is 0.057 (194/3,421). However, the observed overlap between just the TKO negatively affected group and HP1β negatively affected group is 0.175 (84/481), representing a strong multiple of the expected ratio. This multiple was used for a proportions hypothesis test, producing a *p-value* of less than 1.3×10^{-14}.

Oligonucleotide pair sequences used in PCR and quantitative PCR

Assay	Primer Name	5' to 3' Primer Sequences (Forward, Reverse)
EDI splicing	EDI RT-PCR	AGTATGGTGCGGAGGCCCT, GCGGCCAGGGTCACGATC
	qRT-PCR: EDI inclusion	AACCCAGTCCACAGCTATTCC, GCGGCCAGGGTCACGATC
	qRT-PCR: EDI skipping	CGGTCAACTTCAAGCTATTCC, GCGGCCAGGGTCACGATC
	Endogenous EDI RT-PCR	GACTATTGAAGGCTTGCAGCC, CTTGTGGGTGTGACCTGAGTG
RNA-seq Validations	Zfp444 exon 2	CTCGCCCAGGAGAGTGAG, TGTGCACTTCCGGCTGGAG
	Nfat exon 4	GACAAGCGGTGGTGAGGCA, GCTCTCCACTTGCATAGCCTT
	Zfx exon 2	CCCAGTGCTCCAGAGAAAG, AAATGAGTTTGGTGCTTGTTGTTG
	Mbtps2 exon 2	CCGTCTACCTGGCCGACTT, TGCCAAAGTCTGCATCAGTGTTT
	Exoc1 exon 12	AAAGATGAAGATGACTGGCACC, GAGTTTATTCAGACTAGAAGTTGAT
	Clk4 exon 6	GCGAAGGATATGTTCCAAGACAT, TGCACTCTACAACTTTGCCAAAG
	Prrc exon 31	AAGGCTTCCACTTTGCCGACA, TTTGCTTCCCTCCACCTTGAC
	Slc4 exon 11	GGAGGAGCATGAAGAACGAGT, TTTGCCAGGCCCAGGAGATTT
	Bat3 exon 26	TGGGTCCCTATTATCCAGCA, GCTGTAGTTGGGATCTTCCT
	Tcf7l1 exon 3	TCCAGTGCTACAGTCAAGGAC, ATGAGAGGTGTCAGCGGGT
	Arfip exon 5	GATCACATCTCATGGCTTTGAC, CTTATATGTGTTGAGACTCCATTT
	Klhdc exon 2	ACAGCTCAACCGATTCGTGCA, AGAGAGGGTAGTCTTCGTTATC
	Brd2 exon 4	CCTGAGGTGTCCAATCCCAA, TCCTCTTGATAGTACCCATGTC
	Pex6 exon 15	ACCAACAGACCAGACCTCCT, AGAGAGAATAGAGATCTGCACC
	Ubap exon 28	TGCTGCCTACCCACCTGC, ATCGACGAGAGTGAGGATATC
	Mtmr exon 4	TCAGAGAACTCGGTGCATACC, TCTCTCCTGGAAGCAGGGCT
ChIP	FN promoter	CCCTATGGTGCACTCTCAGT, GACTGTGGGTTCGCAGCG
	EDI exon 2	CCCACCACCAAGACCTACTT, CGCGTCGGCCACCTTCTT
	EDI exon 3	TCCTAAGCCACTGCCTGCT, TTACTGCAGTCTGAACCAGAG
	EDI intron 3a	CCACTGCTTGGTTTCCATTTTC, GTTCACTTTCCCTATGTGTAATTG
	EDI intron 3b	GCAAATCAGCTTTACCACTTCC, ATTTAAAGGTATTCTACCACGATTTG
	EDI exon 4a	CTAAAGGACTGGCATTCACTGA, TCGAGTAGGTCACCCTGTAC
	EDI exon 4b	CCTGAGGATGGAATCCATGAG, ACTGTGTACTCAGAACCCGGT
	EDI intron 4a	GCCCTACTGAATGAATTATGCTTC, TACCATTCCTCTTTAAAGAGGATC
	EDI intron 4b	ACACATTTCTCAGCAAACACTTTC, TCTTGTTGGGCTAGGTGGGT
	EIF6 intron 3	ATGCCCTTAGGACTTGAAGC, TCCAGGTCACTCCCATCATA

EDI Bisulfite Sequencing	EDI minigene exon 5	GTGGATATTATTTAATGTTTAGTTTATTGG, CCACTCAAACTTTATTCAAAAACCAC
	EDI minigene FN promoter	TGTATGAAGAATTTGTTTAGGGTTAGG, (1:1 mix of two primers: AATACTAATAACCCGCCAATACTAAC, AATACTAATAACCCACCAATACTAACTT)
	Endogenous EDI	GATGGTGAAGAAGATATTGTAGAG, ATTTTATTATTTCTTACCATTCCTCTTTAA

Antibodies used in this study

Target Protein	Catalogue Number	Applications	Western Blot Dilution
H3	Abcam, ab1791	ChIP	
H3K36me3	Abcam, ab9050	ChIP	
H3K9me2	Millipore, 17-648	ChIP	
H3K9me3	Abcam, ab8898	ChIP	
hnRNP A2/B1	Abcam, ab6102	WB	1:1,000
HP1α	Abcam, ab109028	WB, IP, ChIP	1:2,000
HP1β	Abcam, ab10478	WB, IP, ChIP	1:2,000
HP1γ	Abcam, ab10480	WB, IP, ChIP	1:2,000
HSC-70	Santa Cruz, sc-7298	WB	1:40,000
Normal rabbit IgG	Santa Cruz, sc-2027	IP, ChIP	
RNA Polymerase II phospho-Ser2	Abcam, ab5095	WB	1:1,000
SF3B1 (SAP155)	MBL, D221-3	WB	1:1,000
SRSF1 (SF2)	Abcam, ab38017	WB	1:1,000
SRSF3 (SRp20)	Invitrogen, 33-4200	WB	1:500
SRSF6 (SRp55)	Santa Cruz, sc-34197	WB	1:200
T7 tag	Novagen, 69522-3	WB	1:20,000

Summary of all deep sequencing samples

Sample	Type	Number of reads	alignment rate / concordant pair alignment rate	Alternative exons identified
RNA-seq statistics				
R1 rep1	single-end, 50 bp	37,934,675	91.50%	10,256
R1 rep2	single-end, 50 bp	107,351,762	74.40%	
TKO rep1	single-end, 50 bp	39,210,945	90.50%	10,569
TKO rep2	single-end, 50 bp	98,159,339	78.80%	
HP1α rep1	paired-end, 101 bp	46,710,032	79.00%	8,191
HP1α rep2	paired-end, 101 bp	34,571,675	79.00%	
HP1β rep1	paired-end, 101 bp	43,930,603	79.00%	7,806
HP1β rep2	paired-end, 101 bp	32,931,379	78.30%	
HP1γ rep1	paired-end, 101 bp	37,399,338	78.80%	7,162
HP1γ rep2	paired-end, 101 bp	28,430,784	78.50%	
R1 HP1α+β+γ rep1	paired-end, 101 bp	36,212,481	78.40%	6,432
R1 HP1α+β+γ rep2	paired-end, 101 bp	43,310,560	43.50%	
TKO HP1α+β+γ rep1	paired-end, 101 bp	37,735,675	78.40%	7,250
TKO HP1α+β+γ rep2	paired-end, 101 bp	33,697,859	78.10%	
BS-seq statistics				
R1 rep1	paired-end, 100 bp	116,502,025	56.00%	-
R1 rep2	paired-end, 100 bp	133,732,068	57.50%	
MNase-seq statistics				
R1 rep1	single-end, 39 bp	137,091,627	95.77%	-
R1 rep2	single-end, 40 bp	147,315,292	81.88%	
R1 rep3	single-end, 36 bp	93,472,350	85.22%	
TKO rep1	single-end, 39 bp	139,504,954	96.06%	
TKO rep2	single-end, 40 bp	158,931,933	78.61%	
TKO rep3	single-end, 36 bp	100,792,512	82.14%	

Supplemental References

Bock, C., Reither, S., Mikeska, T., Paulsen, M., Walter, J., and Lengauer, T. (2005). BiQ Analyzer: visualization and quality control for DNA methylation data from bisulfite sequencing. Bioinformatics 21, 4067-4068.

Hegele, A., Kamburov, A., Grossmann, A., Sourlis, C., Wowro, S., Weimann, M., Will, C.L., Pena, V., Luhrmann, R., and Stelzl, U. (2012). Dynamic protein-protein interaction wiring of the human spliceosome. Molecular cell 45, 567-580.

Katz, Y., Wang, E.T., Airoldi, E.M., and Burge, C.B. (2010). Analysis and design of RNA sequencing experiments for identifying isoform regulation. Nature methods 7, 1009-1015.

Kim, D., Pertea, G., Trapnell, C., Pimentel, H., Kelley, R., and Salzberg, S.L. (2013). TopHat2: accurate alignment of transcriptomes in the presence of insertions, deletions and gene fusions. Genome biology 14, R36.

Krueger, F., and Andrews, S.R. (2011). Bismark: a flexible aligner and methylation caller for Bisulfite-Seq applications. Bioinformatics 27, 1571-1572.

Langmead, B., and Salzberg, S.L. (2012). Fast gapped-read alignment with Bowtie 2. Nature methods 9, 357-359.

Langmead, B., Trapnell, C., Pop, M., and Salzberg, S.L. (2009). Ultrafast and memory-efficient alignment of short DNA sequences to the human genome. Genome biology 10, R25.

Siepel, A., Bejerano, G., Pedersen, J.S., Hinrichs, A.S., Hou, M., Rosenbloom, K., Clawson, H., Spieth, J., Hillier, L.W., Richards, S., et al. (2005). Evolutionarily conserved elements in vertebrate, insect, worm, and yeast genomes. Genome research 15, 1034-1050.

Team, R.D.C. (2006). R: A Language and Environment for Statistical Computing. Vienna, R Foundation for Statistical Computing. First citation in article.

Trapnell, C., Williams, B.A., Pertea, G., Mortazavi, A., Kwan, G., van Baren, M.J., Salzberg, S.L., Wold, B.J., and Pachter, L. (2010). Transcript assembly and quantification by RNA-Seq reveals unannotated transcripts and isoform switching during cell differentiation. Nature biotechnology 28, 511-515.

Wahl, M.C., Will, C.L., and Luhrmann, R. (2009). The spliceosome: design principles of a dynamic RNP machine. Cell 136, 701-718.